Cancer Science
The official journal of the Japanese Cancer Association JCA

Identification of transforming activity of free fatty acid receptor 2 by retroviral expression screening

Hisashi Hatanaka,[1,2] Mamiko Tsukui,[2] Shuji Takada,[1] Kentaro Kurashina,[1,3] Young Lim Choi,[1,4] Manabu Soda,[1] Yoshihiro Yamashita,[1] Hidenori Haruta,[1,3] Toru Hamada,[1,3] Toshihide Ueno,[1] Kiichi Tamada,[2] Yoshinori Hosoya,[3] Naohiro Sata,[3] Yoshikazu Yasuda,[3] Hideo Nagai,[3] Kentaro Sugano[2] and Hiroyuki Mano[1,4,5,6]

Divisions of [1]Functional Genomics, [2]Gastroenterology, [3]Department of Surgery, Jichi Medical University, Tochigi; [4]Department of Medical Genomics, Graduate School of Medicine, The University of Tokyo, Tokyo; [5]CREST, Japan Science and Technology Agency, Saitama, Japan

(Received May 4, 2009/Revised August 22, 2009/Accepted August 30, 2009/Online publication September 24, 2009)

Gallbladder cancer (GBC) is a highly fatal malignancy in humans. Genetic alterations in *KRAS* or *TP53* as well as overexpression of *ERBB2* have been shown to contribute to the development of certain types of GBC. However, many cases of GBC do not harbor such genetic changes, with other transforming events awaiting discovery. We here tried to identify novel cancer-promoting genes in GBC, with the use of a retroviral cDNA expression library. A retroviral cDNA expression library was constructed from a surgically resected clinical specimen of GBC, and was used to infect 3T3 fibroblasts in a focus formation assay. cDNA incorporated into the transformed foci was rescued by PCR. One such cDNA was found to encode free fatty acid receptor 2 (FFAR2), a G protein-coupled receptor for short-chain fatty acids. The oncogenic potential of *FFAR2* was confirmed both *in vitro* with the focus formation assay and by evaluation of cell growth in soft agar as well as *in vivo* with a tumorigenicity assay in nude mice. The isolated *FFAR2* cDNA had no sequence alterations, suggesting that upregulation of *FFAR2* expression may contribute to malignant transformation. Indeed, all of quantitative RT-PCR, *in situ* hybridization, and immunohistochemical analyses showed that the amount of *FFAR2* mRNA and its protein product was increased in digestive tract cancer specimens. Furthermore, short-chain fatty acids potentiated the mitogenic action of FFAR2 in 3T3 cells. Our data thus, for the first time, implicate FFAR2 in carcinogenesis of the digestive tract. (*Cancer Sci* 2010; 101: 54–59)

Gallbladder cancer (GBC) is a highly fatal malignancy in humans, being most prevalent in South America and Asia. In most cases, GBC is not diagnosed until it has reached an advanced stage, when the 5-year survival rate is ~10%.[1,2] In the USA, ~8000 new cases of biliary tract cancer (BTC) are diagnosed each year, with ~4000 of the affected individuals subsequently dying of GBC.[3] Several risk factors have been identified for GBC, including cholelithiasis[4] and anomalous pancreaticobiliary duct junction.[5] Genetic alterations in *KRAS* or *TP53* as well as overexpression of *ERBB2* have been shown to contribute to the development of certain types of GBC. However, many cases of GBC do not harbor such genetic changes, with other transforming events awaiting discovery.

The focus formation assay with 3T3 or RAT1 fibroblasts has been used extensively to screen for transforming genes in various carcinomas.[6] In such screening, genomic DNA is isolated from cancer specimens and used to transfect fibroblasts, potentially resulting in the development of transformed cell foci. However, given that expression of the introduced genes is controlled by their own promoters or enhancers, oncogenes in cancer cells may exert effects in fibroblasts only when their control regions are active in these cells, which is not guaranteed.

Adequate expression of cDNA in fibroblasts can be achieved by placing them under the control of an exogenous promoter fragment. Toward this goal, we have recently established a retroviral cDNA expression library system that is sensitive enough to generate libraries with a high complexity even from small amounts of materials such as clinical specimens.[7–9] With this system, we have successfully discovered a fusion-type protein tyrosine kinase EML4–ALK in non-small cell lung cancer.[7]

In this manuscript, we have applied this technology to a surgically resected clinical specimen of GBC, and used this library to screen for transforming genes in GBC. Unexpectedly, transforming ability has been discovered for free fatty acid receptor 2 (FFAR2, also known as GPR43), which functions as a cellular receptor for short-chain fatty acids (SCFA).[10] Further, tumor-specific expression of FFAR2 has been proven among a panel of clinical specimens for GBC, gastric cancer, and colorectal cancer (CRC) by *in situ* hybridization and immunohistochemical analyses, indicating tumor-promoting activity among digestive tract cancers.

Materials and Methods

Clinical specimens and cells lines. Resected clinical materials were obtained from individuals who underwent surgery at Jichi Medical University Hospital. Written informed consent was obtained from each subject according to the protocols approved by the ethics committees of Jichi Medical University. Mouse 3T3 and BOSC23 cell lines were obtained from American Type Culture Collection (Manassas, VA, USA), and maintained in Dulbecco's modified Eagle medium/F12 (DMEM/F12; Invitrogen, Carlsbad, CA, USA) containing 10% fetal bovine serum (Invitrogen) and 2 mM L-glutamine.

Construction of retroviral cDNA expression library. The retroviral cDNA library was constructed as described previously.[7–9,11] Briefly, first-strand cDNA was synthesized from the RNA with the use of PowerScript reverse transcriptase, the SMART IIA oligonucleotide, and CDS primer IIA (all from Clontech, Mountain View, CA, USA). The resulting cDNA was then amplified by PCR with 5′-PCR primer IIA (Clontech) and PrimeSTAR HS DNA polymerase (Takara Bio, Otsu, Shiga, Japan) for 17 cycles of 98°C for 10 s and 68°C for 6 min. The PCR products were ligated to a BstXI adapter (Invitrogen) and then incorporated into the pMXS retroviral plasmid (kindly provided by T. Kitamura of the Institute of Medical Science, University of Tokyo).

Recombinant retroviruses were produced by introduction of the plasmid library into the packaging cell line BOSC23[12] and were used to infect 3T3 cells in the presence of polybrene (4 μg/mL; Sigma, St Louis, MO, USA). The cells were cultured for 2 weeks, after which transformed foci were isolated, expanded, and subjected to extraction of genomic DNA. Insert

[6]To whom correspondence should be addressed. E-mail: hmano@jichi.ac.jp

doi: 10.1111/j.1349-7006.2009.01348.x

cDNA was recovered from the genomic DNA by PCR with 5′-PCR primer IIA and PrimeSTAR HS DNA polymerase. Amplified products were then ligated to the plasmid pT7Blue-2 (Novagen, Madison, WI, USA) and subjected to nucleotide sequencing.

Transformation assay. For a focus formation assay, recombinant retrovirus was used to infect 3T3 cells for 48 h. The culture medium of 3T3 cells was then changed to DMEM/F12 supplemented with 5% calf serum and 2 mM L-glutamine, and incubated for 2 weeks. To examine anchorage-independent growth in soft agar, 3T3 cells infected with retrovirus were resuspended in culture medium containing 0.4% agar (SeaPlaque GTG agarose; Cambrex, East Rutherford, NJ, USA), and seeded onto a base layer of complete medium containing 0.5% agar. Cell growth was assessed after 3 weeks of incubation.

For an *in vivo* tumorigenicity assay, 3T3 cells (2×10^6) infected with the retrovirus expressing FFAR2 were resuspended in 500 μL PBS, and injected into each shoulder of *nu/nu* BALB/c mice (6 weeks old). Tumor formation was assessed after 3 weeks.

Quantitation with real-time RT-PCR. Oligo(dT)-primed cDNA was synthesized from the clinical specimens with PowerScript reverse transcriptase, and subjected to quantitative PCR with a QuantiTect SYBR Green PCR kit (Qiagen, Valencia, CA, USA) and an amplification protocol consisting of incubations at 94°C for 15 s, 60°C for 30 s, and 72°C for 60 s. Incorporation of the SYBR Green dye into PCR products was monitored in real time with an ABI PRISM 7900HT sequence detection system (Applied Biosystems, Foster City, CA, USA), thereby allowing determination of the threshold cycle (C_T) at which exponential amplification of products begins. The C_T values for cDNA corresponding to the β-actin gene (*ACTB*) and *FFAR2* were used to calculate the abundance of the latter mRNA relative to that of the former. The oligonucleotide primers used for PCR were 5′-CCATCATGAAGTGTGACGTGG-3′ and 5′-GTCCGCCTAGAAGCATTTGCG-3′ for *ACTB* and 5′-CACTCAACGCCAGTCTGGAC-3′ and 5′-TGGCATCCCTTCTCCTTGAC-3′ for *FFAR2*.

In situ hybridization with sense or antisense riboprobes corresponding to the 3′ region (nucleotides 867–1229) of the *FFAR2* cDNA isolated in this study was conducted as described previously.[13]

Immunohistochemistry. Human tissues were fixed in 4% formaldehyde in PBS at room temperature overnight, embedded in paraffin, and sectioned at a thickness of 3 μm. Sections were mounted on glass slides, deparaffinized through three changes of xylene for 4 min each, and rehydrated in distilled water through a series of graded alcohols. For histological evaluation, sections were stained with hematoxylin–eosin solutions. For immunohistochemical experiments, antigenicity was enhanced by boiling the sections in 10 mM citrate buffer (pH 6.0) in a microwave oven for 15 min, and the endogenous peroxidase activity was blocked by incubation in methanol containing 0.3% H_2O_2 for 30 min. After two washes with PBS containing 1% Triton X-100, the sections were preincubated with the blocking buffer (#X0909; Dako, Glostrup, Denmark) in a humidified chamber for 20 min at room temperature, and then incubated with anti-FFAR2 antibody (SP4226P; Acris Antibodies, Schillerstaβe, Herford, Germany) at 4°C overnight. Next, the sections were washed in PBS and incubated with horseradish peroxidase (HRP)-labeled polymers conjugated to goat antirabbit immunoglobulin (#K4003; Dako) at 37°C for 30 min. Color development was carried out by incubating the sections with 3,3-diaminobenzidine tetrahydrochloride (Wako Pure Chemical Industries, Osaka, Japan) as a chromogenic substrate. Finally, the sections were lightly counterstained with hematoxylin, mounted, and viewed under a light microscope.

Cell proliferation assay. Mouse 3T3 cells expressing FFAR2 or not expressing FFAR2 were seeded into 96-well plates at a concentration of 4×10^3 cells/well, and incubated for 24 h with DMEM-F12 medium and 1% charcoal-treated fetal bovine serum (Invitrogen). Cells were further cultured for 48 h with 100 mM sodium acetate or 1 mM sodium butyrate, and were subjected to the cell proliferation assay with the WST-1 reagent (Clontech).

Results

Focus formation assay with a GBC library. To screen for transforming genes in digestive tract cancers, we constructed a retroviral cDNA expression library from a surgically resected GBC specimen, and obtained a total of 3.2×10^5 colony-forming units of independent plasmid clones, from which we randomly selected 20 clones and examined the incorporated cDNA. An insert of ≥500 bp was present in 16 (80%) of the plasmid clones, and the average size of these inserts was 1.48 kbp (data not shown). Infection of mouse NIH 3T3 fibroblasts with the recombinant retroviral library generated a total of 89 transformed foci (Fig. 1a). No foci were obtained for cells infected with the empty virus, whereas numerous foci were readily apparent for cells infected with a virus encoding the v-Ras oncoprotein.

Each focus obtained with the cDNA expression library was isolated, expanded independently, and used to prepare genomic DNA for recovery of retroviral inserts by PCR with the primers used originally to amplify the cDNA in construction of the library.[7] We recovered a total of 45 cDNA fragments by PCR, each of which was subjected to nucleotide sequencing in both directions. Screening of the 45 cDNA sequences against the public nucleotide sequence databases revealed that they corresponded to 19 independent genes (Supporting Information Table S1). To confirm the transforming potential of the isolated cDNA, we ligated each cDNA clone to pMXS and used the resulting retroviruses to infect 3T3 cells. The focus formation assay was carried out for cDNA corresponding to 19 independent genes, revealing reproducible transforming activity for: clone ID #2, corresponding to *ARHGEF1* (GenBank accession number NM_004706); clone ID #6, corresponding to *TBC1D3* (GenBank accession number NM_032258); clone ID #7, corresponding to *FGF4* (GenBank accession number NM_002007); and clone ID #14, corresponding to *FFAR2* (GenBank accession number NM_005306) (Fig. 1b).

FFAR2 as an oncogene. FFAR2 functions as a cellular receptor for SCFA,[10] and is expressed in the digestive tract.[14] It is thought to respond to fatty acids released in the digestive tract, but has not previously been shown to possess transforming potential. We therefore focused on FFAR2 in our subsequent analyses. Given that nucleotide sequencing of clone ID #14 did not reveal any sequence alterations compared to the published cDNA sequence of *FFAR2* (GenBank accession number NM_005306), we hypothesized that overexpression of *FFAR2* might contribute to malignant transformation.

We then assessed the transforming activity of FFAR2 in 3T3 cells with a soft-agar assay. Whereas cells infected with the empty virus did not grow in soft agar, those infected with a virus encoding v-Ras grew readily (Fig. 1b). Cells infected with a virus encoding FFAR2 also formed multiple foci in repeated experiments, indicative of the ability of FFAR2 to confer the property of anchorage-independent growth on 3T3 cells. We further tested the activity of FFAR2 in an *in vivo* tumorigenicity assay with athymic nude mice. 3T3 cells infected with the empty virus or with retroviruses encoding FFAR2 or v-Ras were thus injected subcutaneously into the mice. Tumor formation was readily apparent for the cells expressing FFAR2 or v-Ras (Fig. 1b).

Overexpression of FFAR2 in digestive tract cancers. Given that our data revealed an unexpected transforming potential of FFAR2 (at least, when it is abundantly expressed), we examined

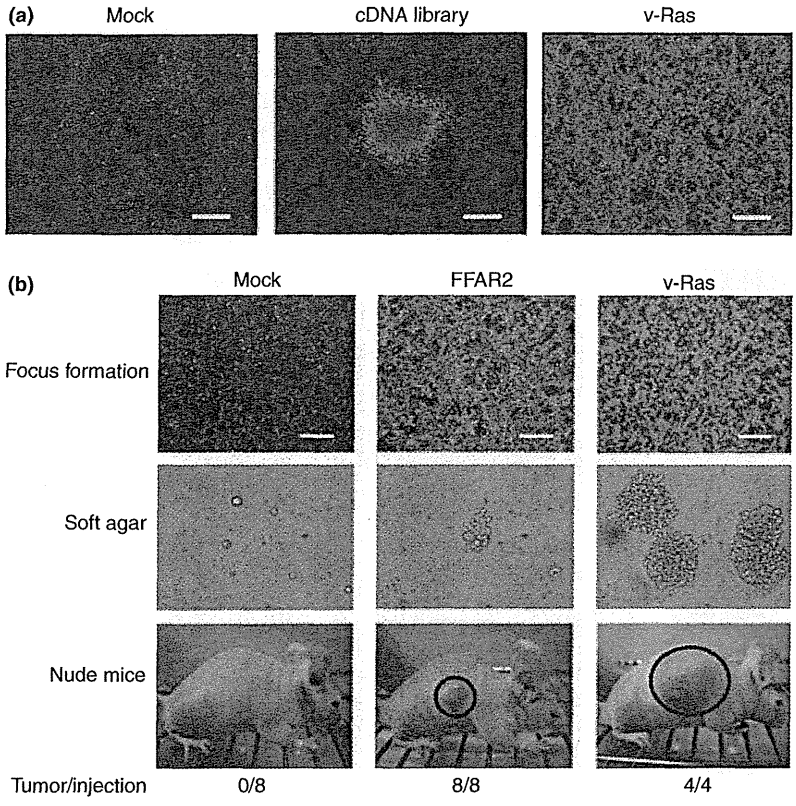

Fig. 1. Transforming activity of free fatty acid receptor 2 (FFAR2). (a) A retroviral cDNA expression library was constructed from a gallbladder cancer specimen isolated from a 64-year-old man. Mouse 3T3 cells were infected with the retroviral cDNA library, a virus encoding v-Ras, or the empty virus (Mock), and were photographed after culture for 2 weeks for the analysis of focus formation. Scale bars = 1 mm. (b) 3T3 cells were infected with viruses encoding FFAR2 or v-Ras or with the empty virus (Mock) and were then cultured for 5 days for analysis of focus formation (top panels: scale bars = 1 mm). The same batches of 3T3 cells were also assayed for anchorage-independent growth in soft agar over 17 days (middle panels) and for tumorigenicity in nude mice over 3 weeks (bottom panels). Tumors formed in the shoulders of mice injected subcutaneously with 1×10^5 cells are indicated by red circles. The frequency of tumor formation (tumor/injection) is also indicated.

whether FFAR2 might be overexpressed in human cancer specimens. We prepared oligo(dT)-primed cDNA from seven specimens of BTC, 89 specimens of gastric cancer, and 80 specimens of CRC by reverse transcription and then subjected the cDNA preparations to quantitative PCR analysis in order to measure the amount of *FFAR2* cDNA. For comparison, we also analyzed specimens of normal gallbladder ($n = 6$) and biliary duct ($n = 1$) as well as paired noncancerous tissue for all specimens of gastric cancer and CRC. Whereas the mean expression level of *FFAR2* seemed higher in BTC compared to normal gallbladder/biliary duct, a large standard deviation in the expression level made the difference insignificant ($P > 0.05$) (Fig. 2a). However, the *FFAR2* level was significantly increased ($P < 0.05$) in gastric cancer (Fig. 2b) and CRC (Fig. 2c) compared with the corresponding paired normal tissue specimens.

To examine further the site and extent of *FFAR2* expression, we carried out *in situ* hybridization analysis with a series of cancer specimens. First, a section of a CRC specimen was subjected to hybridization with sense or antisense probe for *FFAR2* mRNA. Only the antisense probe yielded clear signals in the cytoplasm and nucleus of the cancer cells (Fig. 3a), thus confirming the specificity of this probe. A series of cancer specimens was then subjected to hybridization with the antisense probe for *FFAR2* mRNA. GBC cells exhibited an increased level of hybridization compared with the normal cells in the same section (Fig. 3b). However, epithelial cells of normal gall-

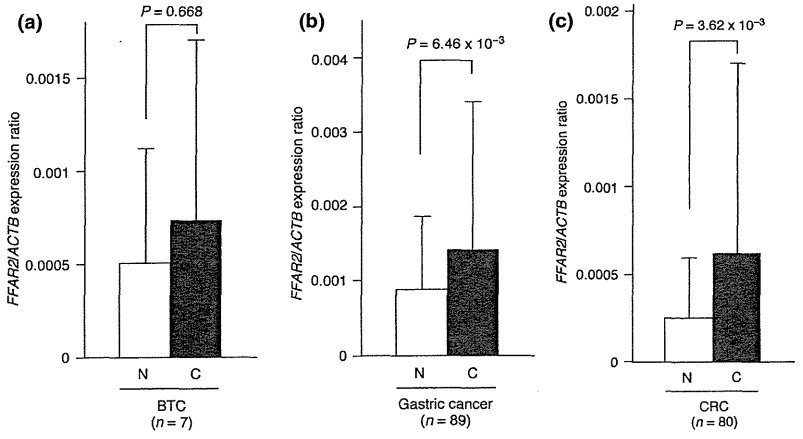

Fig. 2. Expression of free fatty acid receptor 2 (*FFAR2*) in digestive tract cancers. Oligo(dT)-primed cDNA was synthesized from (a) clinical specimens of biliary tract cancer (C) or normal gallbladder and biliary tract tissue (N), or from paired cancerous (C) and noncancerous (N) tissue specimens from patients with (b) gastric cancer or (c) colorectal cancer. The resultant cDNA was subjected to quantitative PCR analysis. Data are means + SD for the indicated *n* values, and *P*-values for the indicated comparisons were determined by Student's *t*-test. ACTB, β-actin.

doi: 10.1111/j.1349-7006.2009.01348.x

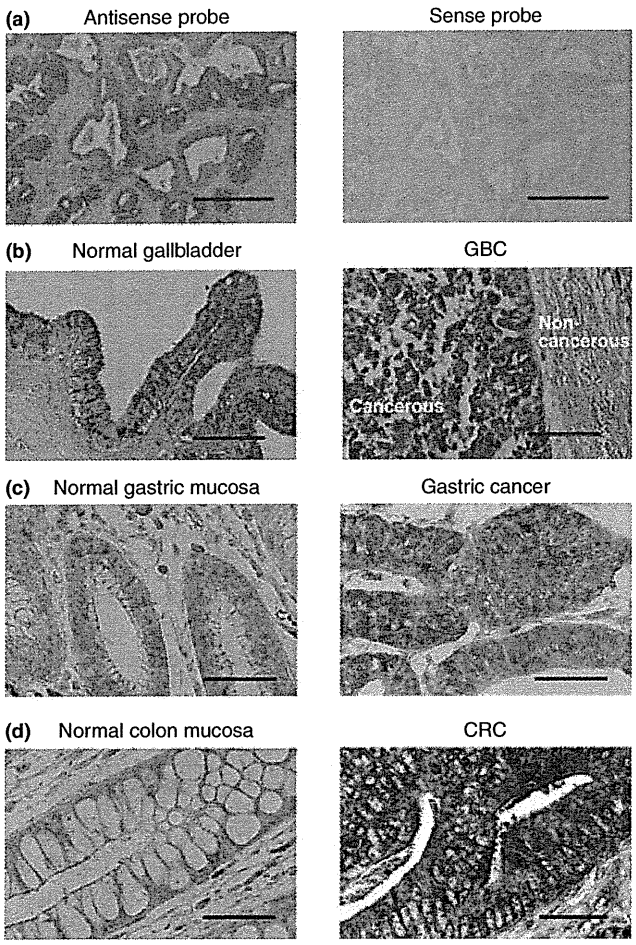

Fig. 3. *In situ* hybridization analysis of free fatty acid receptor 2 (*FFAR2*) expression. (a) A section of colorectal cancer (CRC) was subjected to *in situ* hybridization with sense or antisense riboprobes corresponding to the 3′ region (nucleotides 867–1229) of the *FFAR2* cDNA isolated in this study. (b–d) Sections of (b) normal gallbladder and gallbladder cancer (GBC), (c) paired normal gastric mucosa and gastric cancer, and (d) paired normal colon mucosa and CRC were also subjected to *in situ* hybridization with the antisense probe for *FFAR2* mRNA. Scale bars = 1 mm (a), 100 μm (b), or 50 μm (c,d).

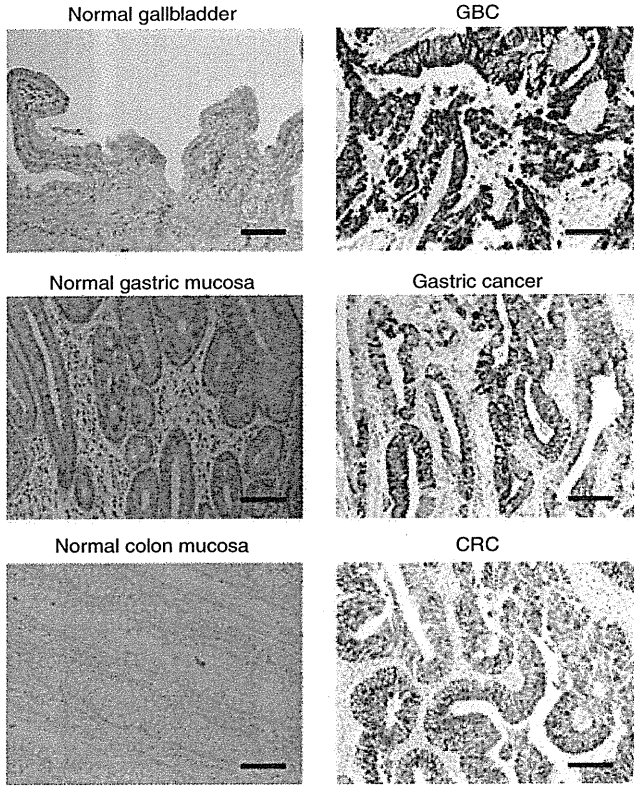

Fig. 4. Immunohistochemical analysis of free fatty acid receptor 2 (FFAR2) expression. Sections of normal gallbladder and gallbladder cancer (GBC) (upper panel), of paired normal gastric mucosa and gastric cancer (middle panel), and of paired normal colon mucosa and colorectal cancer (CRC) (lower panel) were subjected to immunohistochemical staining with antibody to FFAR2. Scale bars = 100 μm.

bladder were also stained with the probe, possibly explaining why the amount of *FFAR2* mRNA did not differ significantly between GBC and normal tissue by quantitative RT-PCR analysis (Fig. 2a). In contrast, the hybridization signal for *FFAR2* mRNA was markedly greater both in gastric cancer cells in eight of 10 specimens examined than in gland cells of the normal stomach (Fig. 3c), as well as in CRC cells in 13 of 14 specimens examined compared with the corresponding normal cells (Fig. 3d), consistent with the data obtained by quantitative RT-PCR analysis (Fig. 2b,c).

Additionally, we further examined the FFAR2 protein level by immunohistochemistry with anti-FFAR2 antibody among digestive tract cancers. As shown in Figure 4, FFAR2 was apparently induced in a GBC specimen (from which the cDNA library was generated) compared to normal gallbladder, in a gastric cancer specimen compared to its paired normal mucosa, and in a CRC specimen compared to the paired normal mucosa.

Ligand-mediated mitogenic signals of FFAR2. Given that SCFA are the presumptive ligands for FFAR2, we next examined whether the transforming activity of FFAR2 might be stimulated by its binding of such ligands. Toward this end, we incubated 3T3 cells expressing *FFAR2* cDNA in the absence or presence of the SCFA sodium acetate or sodium butyrate. Forced expression of FFAR2 induced a small increase in the growth rate of 3T3 cells even in the absence of the SCFA, whereas the SCFA had no effect on the growth of cells not expressing FFAR2. In contrast, sodium acetate (100 mM) induced a pronounced increase in the growth rate of cells expressing FFAR2 (Fig. 5a). A smaller but still significant increase in the growth rate of cells expressing FFAR2 was also induced by the addition of 1 mM sodium butyrate (Fig. 5b).

Discussion

In this study, we constructed a retroviral cDNA expression library for a GBC specimen and thereby identified the transforming potential of FFAR2. In response to its activation by ligand, FFAR2 regulates lipogenesis,[14] neutrophil migration,[15] and intestinal motility.[16] Although SCFA activate the p38 mitogen-activated protein kinase and heat shock protein 27 signaling pathway via FFAR2 in MCF-7 human breast cancer cells,[17] a relationship between FFAR2 and carcinogenesis has not previously been described.

The *FFAR2* gene has been shown to be preferentially expressed in stomach, small intestine, colon, spleen, and adipose tissue of mice.[14] A substantial amount of *FFAR2* mRNA was also detected in the rat gut, with the highest levels apparent in the colon and lower levels observed in esophagus and stom-

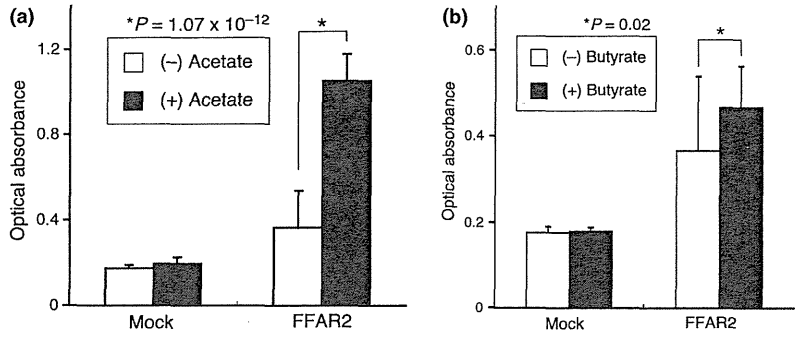

Fig. 5. Effect of short chain fatty acids on the proliferation of cells expressing free fatty acid receptor 2 (FFAR2). Mouse 3T3 cells infected with a virus encoding FFAR2 or with the empty virus (Mock) were cultured for 48 h in DMEM-F12 medium supplemented with 1% charcoal-treated fetal bovine serum in the absence or presence of (a) 100 mM sodium acetate or (b) 1 mM sodium butyrate. Cell proliferation was then assayed with the use of the WST-1 reagent. Data are expressed as absorbance at 450 nm and are means + SD of values from three independent experiments. *P*-values for the indicated comparisons were determined by Student's *t*-test.

ach.[16] In addition, FFAR2 has been detected in enterocytes of the rat intestine[18] as well as in those of the human colon.[19] The preferential expression of FFAR2 in the digestive tract and the mitogenic activity of the encoded protein together suggest a possible role for FFAR2 in carcinogenesis of the digestive system.

In our current analyses, both mRNA and protein amounts for *FFAR2* were frequently induced among the specimens for digestive tract cancer. However, DNA quantitation of the *FFAR2* locus failed to detect copy number changes of the genome (data not shown), and there are no CpG islands mapped closely or within the *FFAR2* locus in the human genome. Therefore, the molecular mechanism underlying such *FFAR2* induction is yet to be revealed.

SCFA, such as acetate, propionate, and butyrate, are the major products of the breakdown of dietary fiber by bacterial fermentation in the mammalian small and large intestine.[20] Among various SCFA, acetate has the highest selectivity for FFAR2.[21] The composition of SCFA in the colonic lumen is ~60% acetate, ~20% propionate, and ~20% butyrate.[22] SCFA are the major anions, being present at a total concentration of ~100 mM, in the lumen of the large intestine in mammals.[23] We found that the mitogenic effect of acetate in 3T3 cells expressing FFAR2 was maximal at ~100 mM (data not shown). These data suggest that FFAR2 may induce mitogenesis in the digestive tract in a manner dependent on the content of SCFA (especially that of acetate) in the diet.

It should be noted that a mere overexpression of FFAR2 significantly induced the growth of 3T3 cells even without the SCFA stimulation (Fig. 5). Although this observation potentially indicates a novel, SCFA-independent function of FFAR2, overexpression of cell surface receptors often stimulates their intracellular signaling with suboptimal concentrations of cognate ligands. Therefore, it is also possible that highly abundant FFAR2 proteins have evoked a mitogenic signaling in 3T3 in response to a low level of SCFA in the serum (or even independent of SCFA).

Diet has a substantial impact on the occurrence of digestive tract cancers, including GBC, gastric cancer, and CRC,[24] as well as on that of chronic inflammatory bowel diseases.[25] Our present findings suggest a possible connection between such disorders and either continuous exposure to SCFA in certain types of diet or induced expression of FFAR2 in the digestive tract. FFAR2 is thus a potential therapeutic target for these disorders.

Acknowledgments

We thank K. Sasaki for technical assistance and T. Kitamura (Institute of Medical Science, University of Tokyo) for the pMXS retroviral plasmid. This study was supported in part by Grants-in-Aid for Scientific Research from the Ministry of Education, Culture, Sports, Science, and Technology, Japan, and by grants from the Japan Society for the Promotion of Science, and from the Ministry of Health, Labour, and Welfare, Japan. The nucleotide sequence of the *FFAR2* cDNA isolated in this study has been deposited in DDBJ/GenBank under the accession number AB378083.

Abbreviations

ALK	anaplastic lymphoma kinase
EML4	echinoderm microtubule associated protein like-4
ERBB2	v-erb-b2 avian erythroblastic leukemia viral oncogene homolog 2
KRAS	v-ki-ras2 Kirsten rat sarcoma viral oncogene homolog
TP53	tumor protein p53

References

1 Carriaga MT, Henson DE. Liver, gallbladder, extrahepatic bile ducts, and pancreas. *Cancer* 1995; **75**: 171–90.
2 Cubertafond P, Gainant A, Cucchiaro G. Surgical treatment of 724 carcinomas of the gallbladder. Results of the French Surgical Association Survey. *Ann Surg* 1994; **219**: 275–80.
3 Jemal A, Siegel R, Ward E, Murray T, Xu J, Thun MJ. Cancer statistics, 2007. *CA Cancer J Clin* 2007; **57**: 43–66.
4 Zatonski WA, Lowenfels AB, Boyle P *et al.* Epidemiologic aspects of gallbladder cancer: a case–control study of the SEARCH Program of the International Agency for Research on Cancer. *J Natl Cancer Inst* 1997; **89**: 1132–8.
5 Hasumi A, Matsui H, Sugioka A *et al.* Precancerous conditions of biliary tract cancer in patients with pancreaticobiliary maljunction: reappraisal of nationwide survey in Japan. *J Hepatobiliary Pancreat Surg* 2000; **7**: 551–5.
6 Goldfarb M, Shimizu K, Perucho M, Wigler M. Isolation and preliminary characterization of a human transforming gene from T24 bladder carcinoma cells. *Nature* 1982; **296**: 404–9.
7 Soda M, Choi YL, Enomoto M *et al.* Identification of the transforming *EML4–ALK* fusion gene in non-small-cell lung cancer. *Nature* 2007; **448**: 561–6.
8 Hatanaka H, Takada S, Choi YL *et al.* Transforming activity of purinergic receptor P2Y, G-protein coupled, 2 revealed by retroviral expression screening. *Biochem Biophys Res Commun* 2007; **356**: 723–6.
9 Choi YL, Kaneda R, Wada T *et al.* Identification of a constitutively active mutant of JAK3 by retroviral expression screening. *Leuk Res* 2007; **31**: 203–9.
10 Brown AJ, Goldsworthy SM, Barnes AA *et al.* The Orphan G protein-coupled receptors GPR41 and GPR43 are activated by propionate and other short chain carboxylic acids. *J Biol Chem* 2003; **278**: 11312–9.
11 Fujiwara S, Yamashita Y, Choi YL *et al.* Transforming activity of purinergic receptor P2Y, G protein coupled, 8 revealed by retroviral expression screening. *Leuk Lymphoma* 2007; **48**: 978–86.
12 Pear WS, Nolan GP, Scott ML, Baltimore D. Production of high-titer helper-free retroviruses by transient transfection. *Proc Natl Acad Sci USA* 1993; **90**: 8392–6.
13 Schaeren-Wiemers N, Gerfin-Moser A. A single protocol to detect transcripts of various types and expression levels in neural tissue and cultured cells: in

doi: 10.1111/j.1349-7006.2009.01348.x

situ hybridization using digoxigenin-labelled cRNA probes. *Histochemistry* 1993; **100**: 431–40.
14 Hong YH, Nishimura Y, Hishikawa D *et al.* Acetate and propionate short chain fatty acids stimulate adipogenesis via GPCR43. *Endocrinology* 2005; **146**: 5092–9.
15 Nilsson NE, Kotarsky K, Owman C, Olde B. Identification of a free fatty acid receptor, FFA2R, expressed on leukocytes and activated by short-chain fatty acids. *Biochem Biophys Res Commun* 2003; **303**: 1047–52.
16 Dass NB, John AK, Bassil AK *et al.* The relationship between the effects of short-chain fatty acids on intestinal motility in vitro and GPR43 receptor activation. *Neurogastroenterol Motil* 2007; **19**: 66–74.
17 Yonezawa T, Kobayashi Y, Obara Y. Short-chain fatty acids induce acute phosphorylation of the p38 mitogen-activated protein kinase/heat shock protein 27 pathway via GPR43 in the MCF-7 human breast cancer cell line. *Cell Signal* 2007; **19**: 185–93.
18 Karaki S, Mitsui R, Hayashi H *et al.* Short-chain fatty acid receptor, GPR43, is expressed by enteroendocrine cells and mucosal mast cells in rat intestine. *Cell Tissue Res* 2006; **324**: 353–60.
19 Karaki SI, Tazoe H, Hayashi H *et al.* Expression of the short-chain fatty acid receptor, GPR43, in the human colon. *J Mol Histol* 2008; **39**: 135–42.
20 Bergman EN. Energy contributions of volatile fatty acids from the gastrointestinal tract in various species. *Physiol Rev* 1990; **70**: 567–90.
21 Le Poul E, Loison C, Struyf S *et al.* Functional characterization of human receptors for short chain fatty acids and their role in polymorphonuclear cell activation. *J Biol Chem* 2003; **278**: 25481–9.
22 Cummings JH, Pomare EW, Branch WJ, Naylor CP, Macfarlane GT. Short chain fatty acids in human large intestine, portal, hepatic and venous blood. *Gut* 1987; **28**: 1221–7.
23 Topping DL, Clifton PM. Short-chain fatty acids and human colonic function: roles of resistant starch and nonstarch polysaccharides. *Physiol Rev* 2001; **81**: 1031–64.
24 Key TJ, Allen NE, Spencer EA, Travis RC. The effect of diet on risk of cancer. *Lancet* 2002; **360**: 861–8.
25 Reif S, Klein I, Lubin F, Farbstein M, Hallak A, Gilat T. Pre-illness dietary factors in inflammatory bowel disease. *Gut* 1997; **40**: 754–60.

Supporting Information

Additional Supporting Information may be found in the online version of this article:

Table S1. Gallbladder cancer cDNA isolated from 3T3 transformants.

Please note: Wiley-Blackwell are not responsible for the content or functionality of any supporting materials supplied by the authors. Any queries (other than missing material) should be directed to the corresponding author for the article.

Cancer Science
The official journal of the Japanese Cancer Association JCA

Identification of the transforming activity of Indian hedgehog by retroviral expression screening

Hisashi Hatanaka,[1,2] Shuji Takada,[1] Mamiko Tsukui,[2] Young Lim Choi,[1,4] Kentaro Kurashina,[3] Manabu Soda,[1] Yoshihiro Yamashita,[1] Hidenori Haruta,[1] Toru Hamada,[1] Kiichi Tamada,[2] Yoshinori Hosoya,[3] Naohiro Sata,[3] Hideo Nagai,[3] Yoshikazu Yasuda,[3] Kentaro Sugano[2] and Hiroyuki Mano[1,4,5,6]

Divisions of [1]Functional Genomics and [2]Gastroenterology, [3]Department of Surgery, Jichi Medical University, Tochigi; [4]Department of Medical Genomics, Graduate School of Medicine, The University of Tokyo, Tokyo; [5]CREST, Japan Science and Technology Agency, Saitama, Japan

(Received May 10, 2009/Revised August 29, 2009/Accepted September 2, 2009/Online publication September 30, 2009)

To identify novel cancer-promoting genes in biliary tract cancer (BTC), we constructed a retroviral cDNA expression library from a clinical specimen of BTC with anomalous pancreaticobiliary duct junction (APBDJ), and used the library for a focus formation assay with 3T3 fibroblasts. One of the cDNAs rescued from transformed foci was found to encode Indian hedgehog homolog (IHH). The oncogenic potential of IHH was confirmed both *in vitro* with the focus formation assay and *in vivo* with a tumorigenicity assay in nude mice. The isolated *IHH* cDNA had no sequence alterations, suggesting that upregulation of IHH expression may contribute to malignant transformation. Quantitation of *IHH* mRNA among clinical specimens has revealed that the expression level of *IHH* in BTC with APBDJ is higher than that in BTC without APBDJ and than in non-cancerous biliary tissues. Our data thus implicate a direct role of IHH in the carcinogenesis of BTC with APBDJ. (*Cancer Sci* 2010; 101: 60–64)

Biliary tract cancer (BTC) is a highly fatal malignancy in humans, and is prevalent in South American and Asian countries; approximately sixteen thousand people die of BTC every year in Japan.[1] Unfortunately, many BTC cases are diagnosed at advanced clinical stages with a 5-year survival rate of ~10%.[2–4] Several risk factors for BTC have been identified to date, including cholelithiasis,[5] anomalous pancreaticobiliary duct junction (APBDJ),[6] and primary sclerosing cholangitis.[7] Genetic alternations in *KRAS* or *TP53* and/or overexpression of *ERBB2* have been shown to contribute to the development of certain types of BTC. However, many cases with BTC do not harbor any such genetic changes, and other transforming events further await discovery.

The focus formation assay with 3T3 or RAT1 fibroblasts has been extensively used to screen for transforming genes in various carcinomas.[8] In such screening, genomic DNA is isolated from cancer specimens, and used to transfect 3T3 fibroblasts to obtain transformed cell foci. As expression of transfected genes in 3T3 cells in this assay is regulated by their own promoter and enhancer fragments, oncogenes with tissue-specific expression (e.g. those with a blood cell-specific promoter) can not become transcriptionally active in 3T3 cells, and thus can no longer be captured in such a screening system.

To ensure the sufficient expression of oncogenes in 3T3 cells, their transcription should be directly regulated by an exogenous promoter fragment. We have therefore constructed a retroviral cDNA expression library from a surgically operated clinical specimen of BTC with APBDJ, which was subsequently used to infect 3T3 cells. In the preparation of the cDNA library, we further took advantage of the SMART PCR system (Clontech, Mountain View, CA, USA), which preferentially amplifies full-length cDNA. A focus formation assay with the library has resulted in the identification of a transforming Indian hedgehog homolog (*IHH*) cDNA.

Materials and Methods

Focus formation assay with a retroviral library. A recombinant retroviral library was constructed as described previously,[9–12] with minor modifications. In brief, total RNA was extracted from a BTC specimen with APBDJ isolated from a 67-year-old man, who gave informed consent. This study was approved by the ethics committee of Jichi Medical University. First-strand cDNA was synthesized from the RNA with the use of PowerScript reverse transcriptase, the SMART IIA oligonucleotide, and CDS primer IIA (all from Clontech). The resulting cDNA was then amplified by PCR with 5′-PCR primer IIA (Clontech) and PrimeSTAR HS DNA polymerase (Takara Bio, Shiga, Japan) for 18 cycles of 98°C for 10 s and 68°C for 6 min. The PCR products were ligated to a *Bst*XI adapter (Invitrogen, Carlsbad, CA, USA) and then incorporated into the pMXS retroviral plasmid (kindly provided by T. Kitamura of the Institute of Medical Science, University of Tokyo). A total of 5.8×10^5 colony forming units of independent plasmid clones was thus generated. Twenty clones were randomly isolated from the library, and examined for the incorporated cDNA. Sixteen (80%) out of the 20 clones contained cDNA inserts with an average length of 1.16 kbp. Recombinant retroviruses were produced by introduction of the plasmid library into the packaging cell line BOSC23 (American Type Culture Collection, Manassas, VA, USA) and were used to infect 3T3 cells in the presence of 4 μg/mL polybrene (Sigma, St Louis, MO, USA). The cells were cultured for 2 weeks, after which transformed foci were isolated, expanded, and subjected to extraction of genomic DNA. Insert cDNA was recovered from the genomic DNA by PCR with 5′-PCR primer IIA and PrimeSTAR HS DNA polymerase. Amplified products were then ligated to the plasmid pT7Blue-2 (Novagen, Madison, WI, USA) and subjected to nucleotide sequencing.

Tumorigenicity assay in nude mice. 3T3 cells (2×10^6) were infected with a retrovirus expressing IHH, resuspended in 500 μL PBS, and injected into each shoulder of a *nu/nu* Balb-c mouse (6 weeks old). Tumor formation was assessed after 2 weeks.

Anchorage-independent growth in soft agar. 3T3 cells (2×10^6) were infected with a retrovirus encoding IHH or v-Ras, resuspended in the culture medium supplemented with 0.4% agar (Sea Plaque GTG agarose; Cambrex, East Rutherford, NJ, USA), and seeded onto a base layer of complete medium supplemented with 0.5% agar. Cell growth was assessed after culture for 2–3 weeks.

Quantitative RT-PCR analysis. Portions of oligo(dT)-primed cDNA produced by reverse transcription were subjected to PCR with a QuantiTect SYBR Green PCR kit (Qiagen, Valencia, CA, USA) and an amplification protocol comprising incubation at 94°C for 15 s, 60°C for 30 s, and 72°C for 60 s. Incorporation

[6]To whom correspondence should be addressed. E-mail: hmano@jichi.ac.jp

doi: 10.1111/j.1349-7006.2009.01355.x

of the SYBR Green dye into PCR products was monitored in real time with an ABI PRISM 7900HT sequence detection system (Applied Biosystems, Foster City, CA, USA), thereby allowing determination of the threshold cycle (C_T) at which exponential amplification of PCR products begins. The C_T values for cDNA corresponding to the β-actin gene (*ACTB*) and *IHH* were used to calculate the abundance of the latter mRNA relative to that of the former. The oligonucleotide primers used for PCR were 5′-CCATCATGAAGTGTGACGTGG-3′ and 5′-GTCCGCCTAGAAGCATTTGCG-3′ for *ACTB* and 5′-CCTCTCTCCTAGAGACCTTG-3′ and 5′-CTGGCTCCCAGGGAATTTAG-3′ for *IHH*.

Immunohistochemistry. Human tissues were fixed in 4% formaldehyde in PBS overnight at room temperature, embedded in paraffin, and sectioned at a thickness of 3 μm. Sections were mounted on glass slides, deparaffinized in three changes of xylene for 4 min each, and rehydrated in distilled water through a series of graded alcohols. For histological evaluation, sections were stained with hematoxylin–eosin. For immunohistochemical experiments, antigenicity was enhanced by boiling the sections in 10 mM citrate buffer (pH 6.0) in a microwave oven for 15 min, and the endogenous peroxidase activity was blocked by incubation in methanol containing 0.3% H_2O_2 for 30 min. After two washes with PBS containing 1% Triton X-100, the sections were preincubated with the blocking buffer (#X0909; Dako, Glostrup, Denmark) in a humidified chamber for 20 min at room temperature, and then incubated overnight at 4°C with anti-IHH antibody (sc-1196; Santa Cruz Biochemistry, Santa Cruz, CA, USA) diluted in PBS. Next, the sections were washed in PBS and incubated with horseradish peroxidase-labeled polymers conjugated to secondary antibodies for primary rabbit antigoat immunoglobulin (Dako, #P0449) without dilution at 37°C for 30 min. Color development was carried out by incubating the sections with 3,3-diaminobenzidine tetrahydrochloride (Wako Pure Chemical Industries, Osaka, Japan) as the chromogenic substrate. Finally, the sections were lightly counterstained with hematoxylin, mounted, and viewed under a light microscope. For the negative control, the immunostaining processes were carried out by replacing the primary antibody with PBS.

Results

Screening with the focus formation assay. From the mRNA of a BTC specimen with APBDJ, full-length cDNA was selectively amplified and ligated to a retroviral vector pMXS. From such library plasmids, we generated a recombinant ecotropic retrovirus that was subsequently used to infect mouse 3T3 fibroblasts. Infection experiments were repeated for a total of four times. After 3 weeks of culture, 75 transformed foci were observed. No foci could be found among the cells infected with an empty virus, while numerous foci were easily identified in the cells infected with a virus expressing v-Ras oncoprotein (data not shown).

Table 1. Bile duct cancer cDNA isolated from 3T3 transformants

Clone ID #	Gene symbol	GenBank no.	Presence of full ORF
1	*FAM83H*	NM_198488	No
2	*GATAD1*	NM_021167	Yes
3	*RRAS2*	NM_012250	No
4	*FASTK*	NM_006712	Yes
5	*VAT1*	NM_006373	Yes
6	*ARPC2*	NM_005731	No
7	*IHH*	NM_002181	Yes
8	*SENP6*	NM_015571	Yes
9	*DOT1L*	NM_032482	ND
10	*LTBR*	NM_002342	ND
11	*KRAS*	NM_004985	Yes
12	*TMEM54*	NM_033504	Yes
13	*RNASET2*	NM_003730	Yes
14	*RPS4X*	NM_001007	Yes
15	*TETRAN*	NM_001120	Yes
16	*DFNB31*	NM_015404	No
17	*CLDN3*	NM_001306	No
18	*GJB2*	NM_004004	Yes
19	*PSMA7*	NM_002792	Yes
20	*PRPSAP1*	NM_002766	Yes
21	*LRRC59*	NM_018509	Yes
22	*LRP5*	NM_002335	ND
23	*NCOR2*	NM_006312	No
24	*KLF16*	NM_031918	No
25	*ARHGAP4*	NM_001666	ND
26	*KIAA0284*	NM_015005	No
27	*DNAJC4*	NM_005528	ND
28	*NOTCH2NL*	NM_203458	No
29	*BCKDHB*	NM_000056	Yes

ND, not determined; ORF, open reading frame.

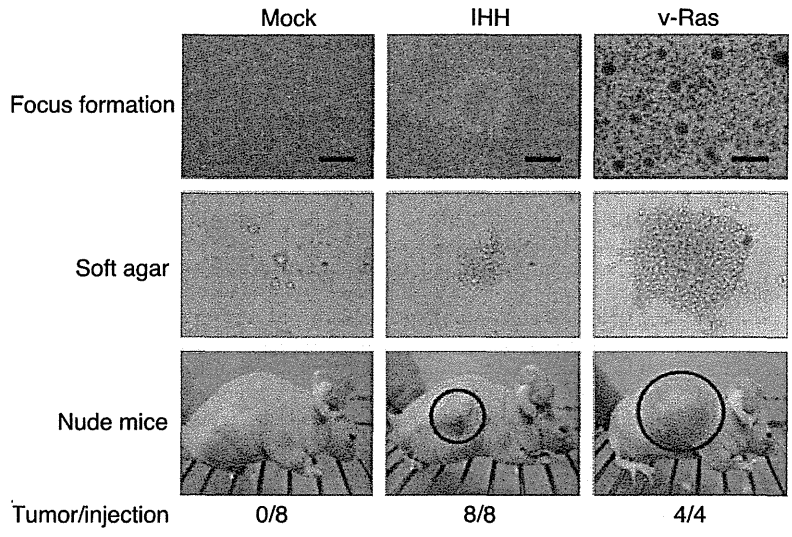

Fig. 1. Transforming activity of Indian hedgehog homolog (IHH). Mouse 3T3 cells were infected with viruses encoding IHH or v-Ras or with the empty virus (Mock), and were then cultured for 5 days for the analysis of focus formation (top panels; scale bars = 1 mm). The same batches of 3T3 cells were also assayed for anchorage-independent growth in soft agar over 17 days (middle panels) and for tumorigenicity in nude mice over 3 weeks (bottom panels). Tumors formed in the shoulders of mice injected subcutaneously with 1×10^5 cells are indicated by red circles. The frequency of tumor formation (tumors/injection) is also indicated.

Each focus was isolated, expanded independently, and used to prepare genomic DNA. We then tried to recover retroviral inserts from such genomic DNA by PCR amplification with the primer used originally to amplify the cDNA in the construction of the library. In most cases, one to three DNA fragments were recovered from each genome, implying multiple retroviral infection of some 3T3 cells.

We finally obtained a total of 44 cDNA fragments by PCR, each of which was ligated into a cloning vector, and subjected to nucleotide sequencing from both ends. Screening of the 44 cDNA sequences against the public nucleotide sequence databases revealed that the 44 fragments correspond to 29 independent genes (Table 1).

Identification of IHH. To confirm the transforming potential of the isolated cDNA, each cDNA clone was ligated to pMXS, and corresponding retrovirus was used to re-infect 3T3 cells. Focus formation assays were conducted for 13 independent genes, discovering a reproducible transforming activity for clone ID #7 corresponding to *IHH* (GenBank accession number, NM_002181) (Fig. 1, top panel). Again, infection with a virus for v-Ras induced many transformed foci, while an empty virus failed to do so. The entire coding region of our ID #7 cDNA was sequenced, revealing no point mutations or deletions compared to the published *IHH* cDNA sequence. Although activation of Hedgehog (Hh) pathways has been revealed among a wide range of digestive tract cancers,[13] oncogenic activity of *IHH* has not been reported to date. We supposed from our data that overexpression of *IHH* may contribute directly to malignant transformation.

Confirmation of the transforming activity of IHH. To confirm the oncogenic activity of IHH, we examined its effect on the anchorage-independent growth of 3T3 cells in soft agar. Whereas cells infected with an empty virus did not grow in the agar, those infected with a virus expressing IHH formed multiple foci in repeated experiments (Fig. 1, middle panel). In addition, 3T3 cells expressing v-Ras readily grew in the agar.

The transforming activity of IHH was also tested by the tumor formation assay with athymic nude mice. 3T3 cells infected with the empty virus or retrovirus expressing IHH or v-Ras were inoculated subcutaneously into nude mice. As shown in the bottom panel of Fig. 1, tumor formation was readily observed for the cells expressing IHH or v-Ras. These results clearly revealed

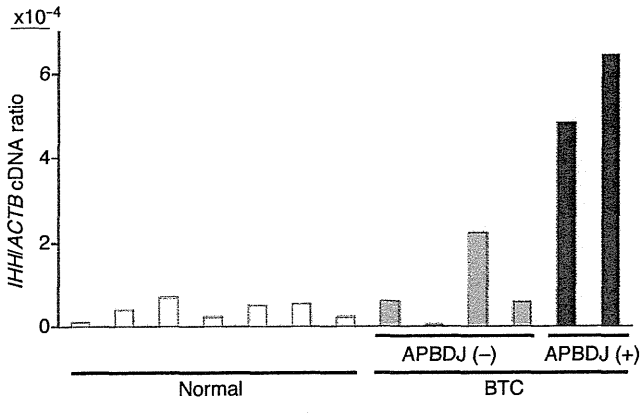

Fig. 2. Expression of Indian hedgehog homolog (*IHH*) in biliary tract. Oligo(dT)-primed cDNA was synthesized from clinical specimens of biliary tract cancer (BTC) with (+) or without (−) anomalous pancreaticobiliary duct junction (APBDJ), or from normal gallbladder (Normal), and were subjected to quantitative PCR analysis for cDNA of *IHH* and β-actin (*ACTB*). The relative expression level of the former to the latter is represented.

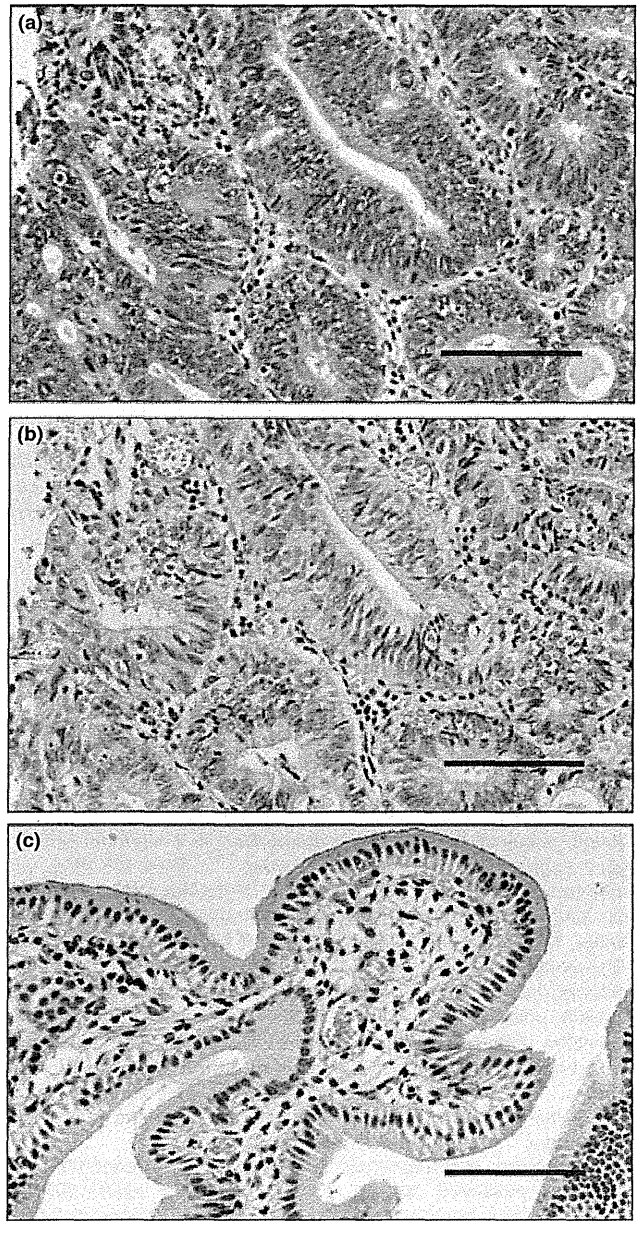

Fig. 3. Immunohistochemical detection of Indian hedgehog homolog (IHH). Expression of IHH is elevated in (a) biliary tract cancer with anomalous pancreaticobiliary duct junction, but such reactivity was absent in the control experiment for (b) the same specimen or (c) anti-IHH staining in normal gallbladder. Scale bars = 100 μm.

an unexpected, direct transforming potential of IHH in fibroblasts.

Overexpression of *IHH* mRNA. Given the transforming potential of wild-type IHH (when it is abundantly expressed), we tried to examine if *IHH* is overexpressed in BTC specimens. Real-time RT-PCR analysis for the quantitation of *IHH* cDNA among normal gall bladder ($n = 7$) and BTC specimens ($n = 6$) (Supporting Information Table S1) revealed that *IHH* is indeed overexpressed in the latter specimens, albeit with marginal statistical significance ($P = 0.06$) by a two-tailed t-test (Fig. 2). It should be noted, however, that BTC cases with APBDJ ($n = 2$) had significantly abundant expression of *IHH* compared to BTC

doi: 10.1111/j.1349-7006.2009.01355.x

without APBDJ ($P = 0.005$) or to normal gall bladder ($P = 2.4 \times 10^{-6}$). Therefore, it is likely that some types of BTC overexpress IHH.

Protein expression of IHH. To confirm the elevated expression of IHH in BTC, we examined its protein level by an immunohistochemical approach. In accordance with the RT-PCR experiments, IHH protein was abundantly detected only in the cytoplasm of cancerous duct but not in stromal cells for BTC with APBDJ (Fig. 3). We failed to observe such staining in normal gallbladder, suggesting that IHH protein was markedly induced in BTC with APBDJ compared to normal gallbladder.

Discussion

In the present study, we have constructed a retroviral cDNA expression library for a BTC specimen with APBDJ, and unexpectedly revealed the transforming potential of IHH through a focus formation assay with the mouse fibroblast cell line 3T3. As there were no sequence alterations in our isolated *IHH* cDNA, the high expression of IHH is likely to exert its oncogenic activity. Consistent with this notion, expression of *IHH* was indeed activated in BTC with APBDJ.

In our transformation assays for IHH (i.e. focus formation assay, soft agar-growth assay, and nude mouse-tumorigenicity assay) we directly used a highly polyclonal, mass culture of 3T3 cells infected with a retrovirus expressing IHH, without any selection (such as positive selection for neomycin resistance-cells). Repeated confirmation of the transforming potential for IHH in such assays (and not for an empty virus) strongly argues against a hypothesis that an artificial expression of mouse genes adjacent to the retroviral integration sites was responsible for the 3T3 transformation in these experiments.

The Hh signaling pathway was originally described in the development of *Drosophila melanogaster* as a segment polarity gene required for embryonic patterning.[14] There are three vertebrate homologues of Hh: Ihh, Sonic hedgehog (Shh), and Desert hedgehog (Dhh) with similar biological properties among them. Hh signaling is known to play a pivotal role in cell fate decisions,[15] tissue repair,[16] and stem cell self renewal.[17,18] Aberration in such signaling may contribute to sustained cell growth and cancer. Indeed, Hahn *et al.* and Johnson *et al.* revealed that mutations within *PTCH1* (a binding partner of hedgehog) cause a cancer-promoting condition, Gorlin syndrome.[19,20] Further, frequent mutations in Hh signaling components have also been identified among sporadic basal cell carcinoma[21] and medulloblastoma.[22]

In addition, transcriptional activation of Hh components has been demonstrated among a wide range of gastrointestinal tumors, which results from endogenous overexpression of Hh proteins such as IHH and SHH.[13] Despite the lack of gene mutations for the Hh components in these tumors, cyclopamine, a specific inhibitor for SMO, suppresses the growth of tumors positive for elevated Hh signaling, supporting the idea that overexpression of the Hh family of proteins may have a mitogenic function.

Our current data proves for the first time the direct transforming potential of IHH, at least in fibroblasts. Furthermore, apparent overexpression of *IHH* in BTC with APBDJ indicates an important role of IHH especially in this subtype of BTC. In addition to the presence or absence of APBDJ, we also examined the clinicopathological features of the BTC specimens used in our study. As shown in Supporting Information Table S1, none of the TNM stage, clinical stage, KRAS mutation, or Ki-67 index were related to the overexpression of *IHH*. However, because the current cohort size is still small, a larger cohort study is mandatory to examine the clinical features of BTC with high *IHH*.

Although Yang *et al.* reported that treatment with a SMO inhibitor leads to downregulation of *CCND1* and upregulation of *CDKN1A* in a cell line of pancreatic carcinoma,[23] we did not observe such a relationship between *CCND1/CDKN1A* and *IHH* expression (data not shown). However, overexpression of *CCND1* may be more prevalent among BTC than that of *IHH*,[24] suggesting the presence of an IHH-independent regulatory network for *CCND1* in BTC.

APBDJ causes pancreatic fluid regurgitation into the biliary duct, and is found frequently among BTC cases.[25] Because pancreatic fluid is rich in various proteases, frequent regurgitation of such fluid into the biliary tract is likely to cause sustained inflammation in the tract. Because inflammation and tissue repair cause transcriptional activation of the Hh family of soluble factors,[16] it may not be surprising to find an elevated level of *IHH* mRNA in the biliary tract with APBDJ. Given the transforming function of abundant IHH, such overexpression may lead to increased cell cycle of biliary tract cells, and eventually to the generation of BTC. Because a number of chemical inhibitors are under development for the Hh pathways,[26] BTC with APBDJ would be an intriguing candidate for such drugs. Further, it is also tempting to examine the Hh ligand levels among human cancers associated with chronic inflammation or regeneration.

Acknowledgments

This work was supported in part by grants for Research on Human Genome and Tissue Engineering and for Third-Term Comprehensive Control Research for Cancer from the Ministry of Health, Labor, and Welfare of Japan, as well as by a grant for Scientific Research on Priority Areas "Applied Genomics" from the Ministry of Education, Culture, Sports, Science, and Technology of Japan.

Abbreviations

CCND1	cyclin D1
CDKN1A	cyclin-dependent kinase inhibitor 1A
ERBB2	v-erb-b2 avian erythroblastic leukemia viral oncogene homolog 2
KRAS	v-ki-ras2 Kirsten rat sarcoma viral oncogene homolog
PTCH1	Patched, Drosophila, homolog of, 1
TP53	tumor protein p53

References

1 National Cancer Center. *Cancer statistics in Japan 2007 (Website on the internet)*. Tokyo, Japan: National Cancer Center, 2008. [Cited 16 November 2007.] Available from URL: http://www.ganjoho.jp/public/statistics/backnumber/2007_en.html.
2 Carriaga MT, Henson DE. Liver, gallbladder, extrahepatic bile ducts, and pancreas. *Cancer* 1995; **75**: 171–90.
3 Cubertafond P, Gainant A, Cucchiaro G. Surgical treatment of 724 carcinomas of the gallbladder. Results of the French Surgical Association Survey. *Ann Surg* 1994; **219**: 275–80.
4 Shaib Y, El-Serag HB. The epidemiology of cholangiocarcinoma. *Semin Liver Dis* 2004; **24**: 115–25.
5 Zatonski WA, Lowenfels AB, Boyle P *et al.* Epidemiologic aspects of gallbladder cancer: a case-control study of the SEARCH Program of the International Agency for Research on Cancer. *J Natl Cancer Inst* 1997; **89**: 1132–8.

6 Hasumi A, Matsui H, Sugioka A *et al.* Precancerous conditions of biliary tract cancer in patients with pancreaticobiliary maljunction: reappraisal of nationwide survey in Japan. *J Hepatobiliary Pancreat Surg* 2000; **7**: 551–5.
7 Rosen CB, Nagorney DM, Wiesner RH, Coffey RJ Jr, LaRusso NF. Cholangiocarcinoma complicating primary sclerosing cholangitis. *Ann Surg* 1991; **213**: 21–5.
8 Aaronson SA. Growth factors and cancer. *Science* 1991; **254**: 1146–53.
9 Soda M, Choi YL, Enomoto M *et al.* Identification of the transforming *EML4–ALK* fusion gene in non-small-cell lung cancer. *Nature* 2007; **448**: 561–6.
10 Hatanaka H, Takada S, Choi YL *et al.* Transforming activity of purinergic receptor P2Y, G-protein coupled, 2 revealed by retroviral expression screening. *Biochem Biophys Res Commun* 2007; **356**: 723–6.
11 Fujiwara S, Yamashita Y, Choi YL *et al.* Transforming activity of purinergic receptor P2Y, G protein coupled, 8 revealed by retroviral expression screening. *Leuk Lymphoma* 2007; **48**: 978–86.
12 Choi YL, Kaneda R, Wada T *et al.* Identification of a constitutively active mutant of JAK3 by retroviral expression screening. *Leuk Res* 2007; **31**: 203–9.
13 Berman DM, Karhadkar SS, Maitra A *et al.* Widespread requirement for Hedgehog ligand stimulation in growth of digestive tract tumours. *Nature* 2003; **425**: 846–51.
14 Nusslein-Volhard C, Wieschaus E. Mutations affecting segment number and polarity in Drosophila. *Nature* 1980; **287**: 795–801.
15 Ingham PW, McMahon AP. Hedgehog signaling in animal development: paradigms and principles. *Genes Dev* 2001; **15**: 3059–87.
16 Beachy PA, Karhadkar SS, Berman DM. Tissue repair and stem cell renewal in carcinogenesis. *Nature* 2004; **432**: 324–31.
17 Liu S, Dontu G, Wicha MS. Mammary stem cells, self-renewal pathways, and carcinogenesis. *Breast Cancer Res* 2005; **7**: 86–95.
18 Liu S, Dontu G, Mantle ID *et al.* Hedgehog signaling and Bmi-1 regulate self-renewal of normal and malignant human mammary stem cells. *Cancer Res* 2006; **66**: 6063–71.
19 Hahn H, Wicking C, Zaphiropoulous PG *et al.* Mutations of the human homolog of Drosophila patched in the nevoid basal cell carcinoma syndrome. *Cell* 1996; **85**: 841–51.
20 Johnson RL, Rothman AL, Xie J *et al.* Human homolog of patched, a candidate gene for the basal cell nevus syndrome. *Science* 1996; **272**: 1668–71.
21 Reifenberger J, Wolter M, Weber RG *et al.* Missense mutations in SMOH in sporadic basal cell carcinomas of the skin and primitive neuroectodermal tumors of the central nervous system. *Cancer Res* 1998; **58**: 1798–803.
22 Taylor MD, Liu L, Raffel C *et al.* Mutations in SUFU predispose to medulloblastoma. *Nat Genet* 2002; **31**: 306–10.
23 Yang Y, Tian X, Xie X, Zhuang Y, Wu W, Wang W. Expression and regulation of hedgehog signaling pathway in pancreatic cancer. *Langenbecks Arch Surg* 2009; doi. 10.1007/s00423-009-0493-9.
24 Hui AM, Li X, Shi YZ, Takayama T, Torzilli G, Makuuchi M. Cyclin D1 overexpression is a critical event in gallbladder carcinogenesis and independently predicts decreased survival for patients with gallbladder carcinoma. *Clin Cancer Res* 2000; **6**: 4272–7.
25 Kimura K, Ohto M, Saisho H *et al.* Association of gallbladder carcinoma and anomalous pancreaticobiliary ductal union. *Gastroenterology* 1985; **89**: 1258–65.
26 Rubin LL, de Sauvage FJ. Targeting the Hedgehog pathway in cancer. *Nat Rev Drug Discov* 2006; **5**: 1026–33.

Supporting Information

Additional Supporting Information may be found in the online version of this article:

Table S1. Clinical characteristics of the patients with biliary tract cancer (BTC).

Please note: Wiley-Blackwell are not responsible for the content or functionality of any supporting materials supplied by the authors. Any queries (other than missing material) should be directed to the corresponding author for the article.

doi: 10.1111/j.1349-7006.2009.01355.x

Histone deacetylases are critical targets of bortezomib-induced cytotoxicity in multiple myeloma

Jiro Kikuchi,[1] Taeko Wada,[1] Rumi Shimizu,[1] Tohru Izumi,[2] Miyuki Akutsu,[2] Kanae Mitsunaga,[1] Kaoru Noborio-Hatano,[3] Masaharu Nobuyoshi,[3] Keiya Ozawa,[3] Yasuhiko Kano,[2] and Yusuke Furukawa[1,3]

[1]Division of Stem Cell Regulation, Center for Molecular Medicine, Jichi Medical University, Shimotsuke, Tochigi; [2]Division of Hematology, Tochigi Cancer Center, Utsunomiya, Tochigi; and [3]Division of Hematology, Department of Internal Medicine, Jichi Medical University, Shimotsuke, Tochigi, Japan

Bortezomib is now widely used for the treatment of multiple myeloma (MM); however, its action mechanisms are not fully understood. Despite the initial results, recent investigations have indicated that bortezomib does not inactivate nuclear factor-κB activity in MM cells, suggesting the presence of other critical pathways leading to cytotoxicity. In this study, we show that histone deacetylases (HDACs) are critical targets of bortezomib, which specifically downregulated the expression of class I HDACs (HDAC1, HDAC2, and HDAC3) in MM cell lines and primary MM cells at the transcriptional level, accompanied by reciprocal histone hyperacetylation. Transcriptional repression of HDACs was mediated by caspase-8–dependent degradation of Sp1 protein, the most potent transactivator of class I HDAC genes. Short-interfering RNA-mediated knockdown of HDAC1 enhanced bortezomib-induced apoptosis and histone hyperacetylation, whereas HDAC1 overexpression inhibited them. HDAC1 overexpression conferred resistance to bortezomib in MM cells, and administration of the HDAC inhibitor romidepsin restored sensitivity to bortezomib in HDAC1-overexpressing cells both in vitro and in vivo. These results suggest that bortezomib targets HDACs via distinct mechanisms from conventional HDAC inhibitors. Our findings provide a novel molecular basis and rationale for the use of bortezomib in MM treatment. (*Blood.* 2010;116(3):406-417)

Introduction

Despite recent advances in treatment strategies using dose-intensified regimens and new molecular-targeted compounds, multiple myeloma (MM) remains incurable for most patients.[1] To improve their prognosis, the development of molecular-targeted therapy, which involves therapeutic agents with distinct mechanisms of action and high specificity, is highly anticipated. Inhibitors of histone deacetylases (HDACs) and proteasome are promising candidates for these agents, and their clinical efficacy has been reported.[2-4] Moreover, their combinations were proved to be additive in preclinical studies[5,6] and are presently the focus of clinical trials.[7]

Aberrant transcriptional repression of genes regulating cell growth and differentiation is a hallmark of cancer.[8] Recently, evidence has accumulated suggesting that altered activation of HDACs underlies transcriptional repression in malignancies.[9] HDACs are a family of enzymes that catalyze the removal of acetyl groups from core histones, resulting in chromatin compaction and transcriptional repression.[10] HDACs are divided into 5 groups: class I (HDAC1, HDAC2, HDAC3, and HDAC8), class IIa (HDAC4, HDAC5, HDAC7, and HDAC9), class IIb (HDAC6 and HDAC10), class III (SIRT family), and class IV (HDAC11). Class I HDACs are ubiquitously expressed and are generally involved in cell growth and differentiation,[11] whereas class II HDACs have a more restricted pattern of expression (skeletal muscle, heart, and brain) and act in association with tissue-specific transcription factors. In leukemic cells, fusion proteins such as PML/RARα and AML-1/ETO form a complex with HDACs with higher affinities than their normal counterparts, and aberrantly suppress the expression of genes required for cell differentiation and growth control, leading to the transformation of hematopoietic progenitor cells.[12,13] In addition, we have shown that class I HDACs are up-regulated in malignant melanoma and leukemias in association with histone hypoacetylation.[14,15] Similarly, the aberrant expression of HDACs may contribute to the uncontrolled growth of myeloma cells.

Given the role of HDACs in tumor cells, the use of small compounds that inhibit HDAC activity, collectively referred to as HDAC inhibitors, is expected to become a novel strategy for the treatment of cancer.[16] HDAC inhibitors are able to restore the expression of genes that are aberrantly suppressed in tumor cells, which may result in cell-cycle arrest, differentiation, and apoptosis.[17]

The proteasome inhibitor bortezomib (Velcade [Millennium Pharmaceuticals]; formerly known as PS-341) is now widely used for the treatment of MM.[3,4] Bortezomib is a reversible inhibitor of the 26S proteasome complex, which catalyzes ubiquitin-dependent protein degradation. Inhibition of this complex ultimately leads to modulation of the abundance and functions of many intracellular proteins, which may be associated with cytotoxic effects on malignant cells.[18] Recently, novel proteasome inhibitors, which target the ubiquitin-proteasome system in a manner distinct from bortezomib, have been developed and have shown strong activity in preclinical studies.[19,20] These new inhibitors are thought to be promising candidates for MM treatment.

Recent genome-wide approaches have revealed that nuclear factor-κB (NF-κB) is frequently activated in MM cells.[21,22] Because IκBα, which inactivates NF-κB, is a substrate of the

Submitted July 31, 2009; accepted February 23, 2010. Prepublished online as *Blood* First Edition paper, March 29, 2010; DOI 10.1182/blood-2009-07-235663.

An Inside *Blood* analysis of this article appears at the front of this issue.

The online version of this article contains a data supplement.

The publication costs of this article were defrayed in part by page charge payment. Therefore, and solely to indicate this fact, this article is hereby marked "advertisement" in accordance with 18 USC section 1734.

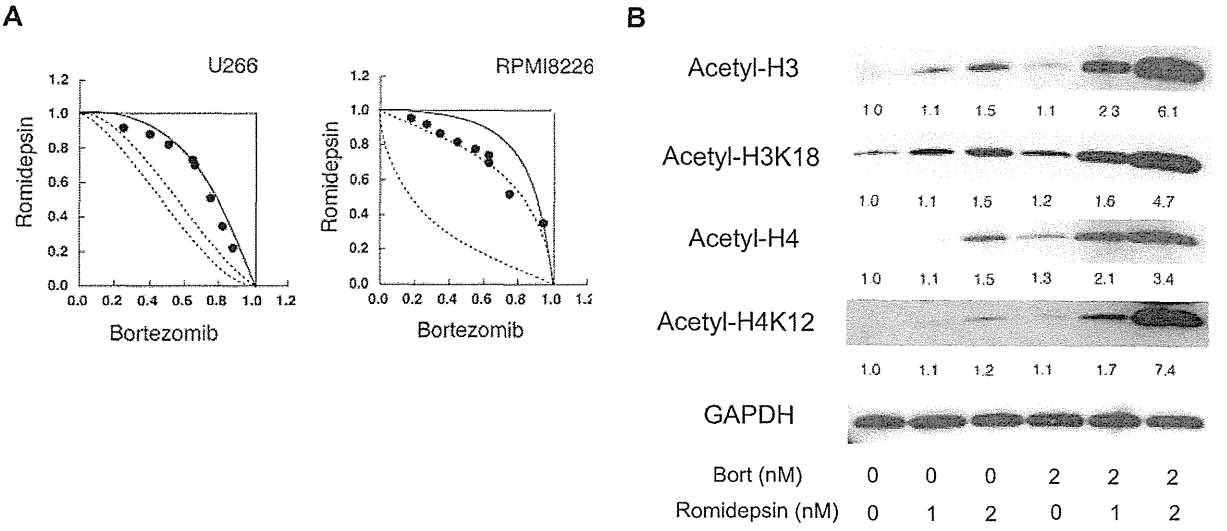

Figure 1. Synergistic effects of romidepsin and bortezomib on cell viability and histone acetylation. (A) Isobolograms of simultaneous exposure of U266 and RPMI8226 cells to bortezomib and romidepsin are shown. The concentrations that produced 80% growth inhibition are expressed as 1.0 on the ordinate and abscissa of isobolograms. The envelope of additivity, surrounded by solid and broken lines, is constructed from dose-response curves of bortezomib and romidepsin. When the data points of the drug combination fall within the area surrounded by the envelope of additivity, the combination is regarded as additive. When the data points fall to the left of the envelope, the drug combination is regarded as supra-additive (synergism). When the data points fall to the right of the envelope, the combination is regarded as antagonistic. The isobolograms shown are representative of at least 3 independent experiments. Each point represents the mean value of at least 3 independent experiments; the SEMs were less than 25% and were omitted. (B) U266 cells were cultured in the absence or presence of either romidepsin (Romidepsin), bortezomib (Bort), or both agents for 48 hours at the indicated doses. Whole-cell lysates were subjected to immunoblotting. The membranes were reprobed with anti-GAPDH antibody to serve as a loading control. The signal intensities of each band were quantified, normalized to those of the corresponding GAPDH, and shown as relative values setting untreated controls to 1.0. Data shown are representative of multiple independent experiments.

proteasome complex, the initial rationale for the use of bortezomib was the inhibition of NF-κB activity.[23] Despite several preclinical studies and clinical trials of MM,[3,4] the inhibition of NF-κB activity has not been demonstrated in bortezomib-treated MM cells. In addition, Hideshima et al[24] recently reported that bortezomib did not inactivate but rather activated the canonical NF-κB pathway in MM cells, suggesting that bortezomib-induced cytotoxicity could not be fully attributed to the inhibition of NF-κB activity. Taken together, there may be other critical pathways and target molecules of bortezomib that have not been fully investigated.

In this study, we found that bortezomib specifically down-regulated the expression of class I HDACs and induced histone hyperacetylation in MM cells. Gain- and loss-of-function analyses revealed that bortezomib-induced cytotoxicity depends on cellular HDAC activities both in vitro and in vivo. Based on these findings, we propose that HDACs are novel critical downstream targets of bortezomib. This finding may provide a novel molecular basis and rationale for the use of bortezomib in MM treatment.

Methods

Cells and cell culture

We used 3 bona fide human MM cell lines, KMS12-BM, RPMI8226, and U266, in this study.[25] These cell lines were purchased from the Health Science Research Resources Bank and maintained in RPMI 1640 medium (Sigma-Aldrich) supplemented with 10% heat-inactivated fetal calf serum (Sigma-Aldrich) and antibiotics. Primary $CD138^+$ MM cells were isolated from the bone marrow (BM) of patients at the time of diagnostic procedure using the magnetic-activated cell sorter (MACS) system (Miltenyi Biotec). Informed consent was obtained in accordance with the Declaration of Helsinki, and the protocol was approved by the institutional review board of Jichi Medical University.

Drugs

Bortezomib and romidepsin (formerly known as FK228 or depsipeptide) were obtained from Millennium Pharmaceuticals and Gloucester Pharmaceuticals, respectively. HDAC6-specific inhibitor tubacin and its inactive derivative niltubacin were provided by Dr Stuart L. Schreiber (Broad Institute of Harvard University and Massachusetts Institute of Technology). We used vincristine (Shionogi Co Ltd), doxorubicin (Meiji Co Ltd), and dexamethasone (Sigma-Aldrich) as conventional antimyeloma drugs. All drugs were dissolved in RPMI 1640 medium at appropriate concentrations and stored at −80°C until use.

Isobologram of Steel and Peckham

The cytotoxic interaction of bortezomib and romidepsin was evaluated at the point of IC_{80} by the isobologram of Steel and Peckham. IC_{80} was defined as the concentration of drugs that produced 80% inhibition of cell growth. The theoretical basis of the isobologram method has been previously described in detail.[26]

Assessment of cell death

Cells were washed with phosphate-buffered saline (PBS) and stained with allophycocyanin-conjugated annexin-V (annexin-V/APC; Biovision). Cell death/apoptosis was judged by annexin-V reactivity and BrdU/7-AAD double-staining using a FACSAria flow cytometer (Becton Dickinson) as described previously.[27]

Immunoblotting

Immunoblotting was carried out according to the standard method using the following antibodies: antiacetyl histone H3, antiacetyl histone H4 (Upstate Biotechnology/Millipore), antiacetyl histone H3–lysine18, antiacetyl histone H4–lysine12, antiacetyl–α-tubulin (Cell Signaling Technology), anti-HDAC1 (Sigma-Aldrich), anti-HDAC2 (MBL International), anti-HDAC3 (BD PharMingen), anti-Sp1, anti–MZF-1, and anti-GAPDH (Santa Cruz Biotechnology).[28]

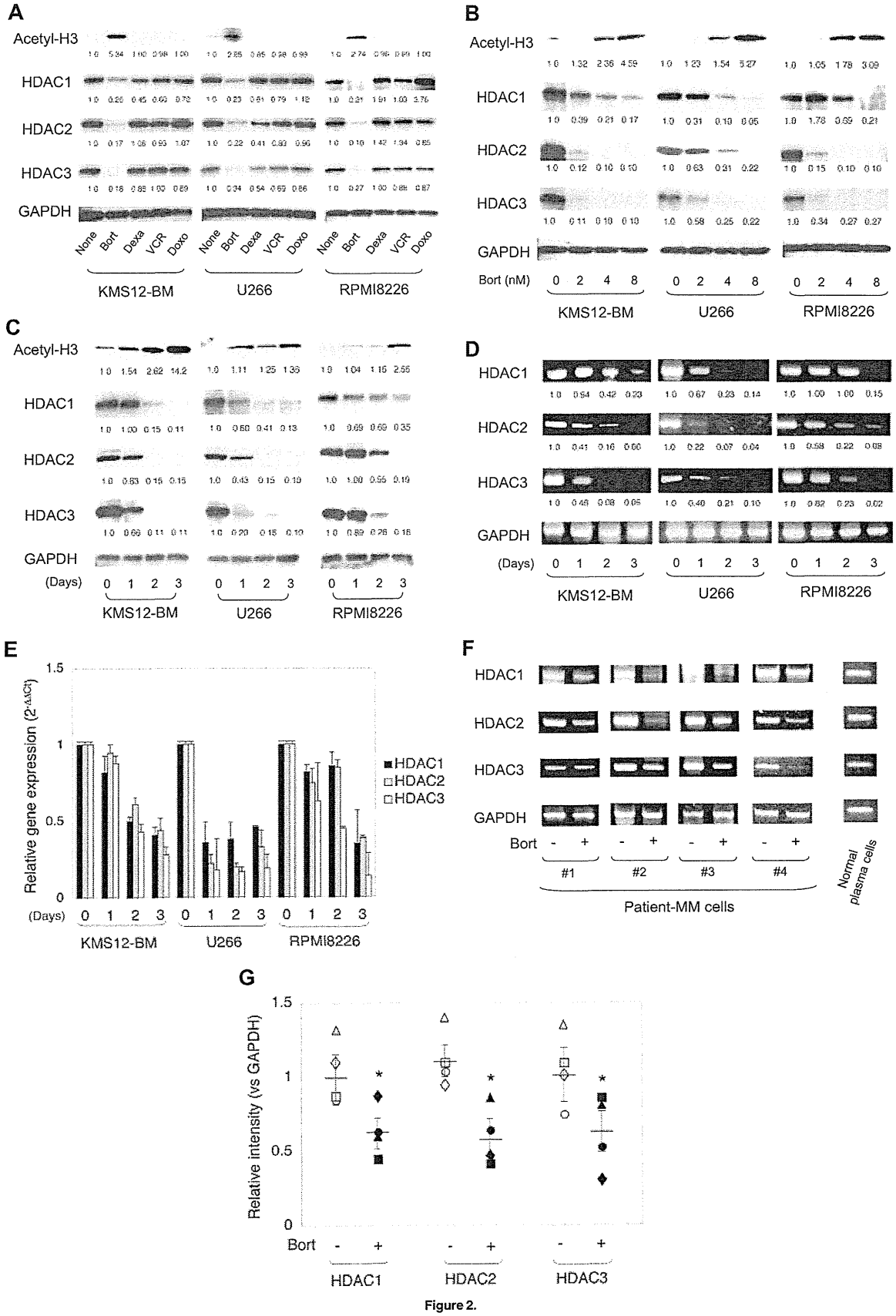
A
Acetyl-H3
HDAC1
HDAC2
HDAC3
GAPDH
None Bort Dexa VCR Doxo
KMS12-BM
U266
RPMI8226
B
Acetyl-H3
HDAC1
HDAC2
HDAC3
GAPDH
Bort (nM) 0 2 4 8
KMS12-BM
U266
RPMI8226
C
Acetyl-H3
HDAC1
HDAC2
HDAC3
GAPDH
(Days) 0 1 2 3
KMS12-BM
U266
RPMI8226
D
HDAC1
HDAC2
HDAC3
GAPDH
(Days) 0 1 2 3
KMS12-BM
U266
RPMI8226
E
Relative gene expression (2^-ΔΔCt)
1.5
1
0.5
0
HDAC1
HDAC2
HDAC3
(Days) 0 1 2 3
KMS12-BM
U266
RPMI8226
F
HDAC1
HDAC2
HDAC3
GAPDH
Bort - + - + - + - +
#1 #2 #3 #4
Patient-MM cells
Normal plasma cells
G
Relative intensity (vs GAPDH)
1.5
1
0.5
0
Bort - + - + - +
HDAC1
HDAC2
HDAC3

Figure 2.

Semiquantitative or real-time quantitative RT-PCR

Total cellular RNA was isolated from 1 to 10×10^4 cells, reverse-transcribed into cDNA using SuperScript reverse transcriptase and oligo(dT) primers (Invitrogen), and subjected to subsequent semiquantitative reverse transcription–polymerase chain reaction (RT-PCR) or real-time quantitative RT-PCR using Power SYBR Green PCR Master Mix (Applied Biosystems) as described previously.[29] Detailed information of primers, including sequences, corresponding nucleotide positions, and PCR product sizes, is shown in supplemental Table 1 (available on the *Blood* Web site; see the Supplemental Materials link at the top of the online article).

Reporter assays

We amplified the promoter region of the HDAC1 gene (−1170 to +397) by PCR and inserted it into the pGL4.10 firefly luciferase vector (Promega) to generate reporter plasmids.[15] We introduced the reporter plasmids into MM cells along with pGL4.73 Renilla luciferase vector (Promega), which served as a positive control to determine transfection efficiencies, in the presence of either test plasmids encoding Sp1 and MZF-1 or empty vectors by electroporation, as previously described.[15] After 48 hours, firefly and Renilla luciferase activities were discriminately measured using the Dual-Luciferase Reporter Assay System (Promega). The promoterless pGL4-basic vector was used as a negative control. The luciferase activity was normalized by the internal standard and indicated as a relative ratio to the negative control. Expression vectors for MZF-1 and Sp1 were kindly provided by Dr Robert Hromas (University of New Mexico) and Dr Mitsuru Nakamura (National Institute of Advanced Industrial Science and Technology), respectively.

ChIP assays

We used the ChIP-IT Chromatin Immunoprecipitation Kit (Active Motif) to perform chromatin immunoprecipitation (ChIP) assays. In brief, cells were fixed with 1% formaldehyde at 37°C for 5 minutes and sonicated to obtain chromatin suspensions. After centrifugation, supernatants were incubated with antibodies of interest at 4°C overnight. The mixture was then incubated with protein A agarose beads at 4°C for 1 hour, and centrifuged to collect the beads. DNA fragments bound to the beads were purified with vigorous washing and subjected to PCR using primer pairs, as shown in supplemental Table 2.[15]

Construction and production of lentiviral expression vectors

We used a lentiviral short-hairpin RNA/short-interfering RNA (shRNA/siRNA) expression vector pLL3.7 for knockdown experiments.[30] siRNA target sequences were designed to be homologous to wild-type cDNA sequences. Oligonucleotides were chemically synthesized, annealed, terminally phosphorylated, and inserted into pLL3.7 vector. Oligonucleotides containing siRNA target sequences are shown in supplemental Table 3. Scrambled sequences were used as controls.

We also used a lentiviral vector CSII-CMV-MCS-IRES-VENUS (kindly provided by Dr Hiroyuki Miyoshi, RIKEN BioResource Center) for gain-of-function experiments after replacing VENUS with DsRed amplified from pDsRed-expressing vector (Clontech Inc).[27] The resulting construct was designated as the CSII-DsRed vector. We constructed HDAC expression vectors by inserting the coding regions of HDAC1, HDAC2, or HDAC3 cDNA (all provided by Dr Stuart L. Schreiber, Broad Institute of Harvard University and MIT).

These vectors were cotransfected into 293FT cells with packaging plasmids (Invitrogen) to produce infective lentiviruses in culture supernatants. Lentiviruses were then added to cell suspensions in the presence of 8 μg/mL polybrene, and transduced for 24 hours, as previously described.[27]

Xenograft murine model

Mice were inoculated subcutaneously in the right thigh with 3×10^7 MM cells in 1×10^{-4} L of RPMI 1640 medium together with 1×10^{-4} L of Matrigel basement membrane matrix (Becton Dickinson).[31] When tumors were measurable, mice were assigned to 3 treatment groups receiving either the vehicle alone (control), bortezomib alone, or bortezomib plus romidepsin. Bortezomib and romidepsin were given intravenously twice a week via the tail vein at 0.5 mg/kg for 4 weeks and intraperitoneally every other day at 0.25 mg/kg for 2 weeks, respectively.[31,32] The control group received the vehicle (0.9% NaCl) alone on the same schedule. Caliper measurements of the longest perpendicular tumor diameters were performed every alternate day to estimate the tumor volume using the following formula: $4/3\pi \times (\text{width}/2)^2 \times (\text{length}/2)$, which represents the 3-dimensional volume of an ellipse.

Results

Synergistic effects of romidepsin and bortezomib on viability and histone acetylation of MM cells

Romidepsin has proved to be one of the most effective HDAC inhibitors against hematologic malignancies both in vitro and in vivo.[33,34] Initially, we examined the combination of romidepsin and bortezomib to develop an effective treatment strategy for MM, because bortezomib can enhance the effects of other anticancer drugs.[6,30] As anticipated, an isobologram analysis of drug combination revealed that bortezomib and romidepsin showed synergistic cytotoxicity in U266 and RPMI8226 cells (Figure 1A). Next, we investigated the molecular basis of the synergistic effect of the 2 drugs. We speculated that bortezomib enhanced the HDAC inhibitory activities of romidepsin. To test this hypothesis, we determined cellular HDAC activity by monitoring the status of histone acetylation. As shown in Figure 1B, consistent with our hypothesis, bortezomib markedly enhanced romidepsin-induced hyperacetylation of histones H3 and H4. Moreover, we found here that bortezomib not only enhanced the effect of romidepsin but also induced histone hyperacetylation. These results suggest a novel mechanism of bortezomib action: it may induce cytotoxicity in MM cells by HDAC suppression. Although most cellular HDAC

Figure 2. Expression of class I HDACs in MM cells during bortezomib treatment. (A) MM cell lines (KMS12-BM, U266, and RPMI8226) were cultured in the absence or presence of either 4nM bortezomib (Bort), 50nM dexamethasone (Dexa), 1nM vincristine (VCR), or 100nM doxorubicin (Doxo) for 48 hours. Whole-cell lysates were subjected to immunoblotting. (B) MM cell lines were cultured in the absence or presence of bortezomib (Bort) at the indicated doses for 48 hours, or (C) cultured in the presence of 4nM bortezomib for up to 3 days. Whole-cell lysates were prepared at given time points and subjected to immunoblotting. (D) Total cellular RNA was isolated simultaneously in the experiments described in panel C and subjected to semiquantitative RT-PCR analysis for the expression of HDAC1, HDAC2, HDAC3, and GAPDH (internal control). The amplified products were visualized by ethidium bromide staining after 2% agarose gel electrophoresis. The results of suboptimal amplification cycles, 35 cycles, are shown. The signal intensities of each band were quantified, normalized to those of the corresponding GAPDH, and shown as relative values setting day 0 controls to 1.0. (E) Total cellular RNA was isolated simultaneously in the experiments described in panel C and subjected to real-time quantitative RT-PCR. The expression of HDAC1, HDAC2, and HDAC3 was normalized to that of GAPDH and quantified by the $2^{-\Delta\Delta Ct}$ method. The means ± SD (bars) of 3 independent experiments are shown. (F) We cultured primary MM cells in the absence or presence of 2nM bortezomib for 48 hours, and determined the expression of HDAC1, HDAC2, HDAC3, and GAPDH (internal control) transcripts by semiquantitative RT-PCR. PCR amplification was carried out with 1 μL of cDNA solution (corresponding to 500 cells). PCR products were resolved on 2% agarose gels and visualized by staining with ethidium bromide. The results of suboptimal amplification cycles, 40 cycles, are shown. (G) The signal intensities of HDACs were quantified with a densitometer, and their means are shown as a ratio to those of GAPDH in corresponding samples. The values of individual samples isolated in the absence or presence of bortezomib are indicated as follows: patient no. 1, circles; patient no. 2, squares; patient no. 3, triangles; and patient no. 4, diamonds, respectively. Bars indicate the average values of each molecule. *P* values were calculated by 1-way analysis of variance (ANOVA) with the Student-Newman-Keuls multiple comparisons test. $^*P < .05$.

activities rely on class I HDACs, Hideshima et al[35] showed that specific inhibitors of class II HDACs, such as tubacin, synergized with bortezomib via inhibition of HDAC6 activity. We therefore examined the effect of romidepsin on HDAC6 activity by monitoring the status of tubulin acetylation. As shown in supplemental Figure 1, tubulin acetylation was observed only at higher concentrations (> 2nM), indicating that romidepsin inhibits the activities of class I HDACs at lower concentrations and both class I and class II HDACs at higher concentrations. As additive cytotoxicity and histone hyperacetylation were observed with less than 1nM romidepsin, these effects are considered to be achieved mainly via the inhibition of class I HDACs. Thereafter, we focused on this novel

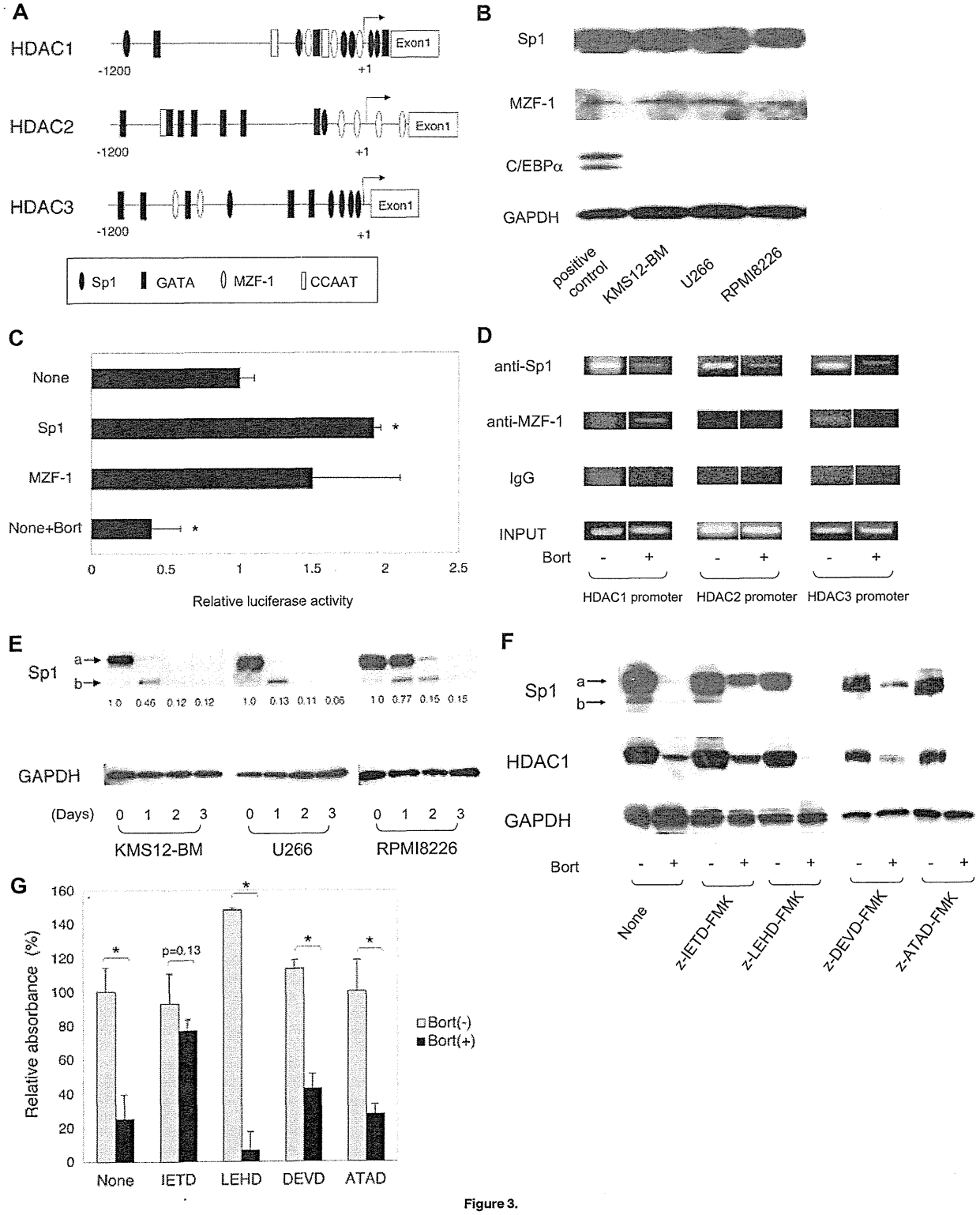

Figure 3.

property of bortezomib and investigated its molecular mechanisms and roles in cytotoxicity against MM.

Down-regulation of HDAC expression in MM cells during bortezomib treatment

First, we investigated the molecular mechanisms of how bortezomib induced histone hyperacetylation in MM cells. We speculated that bortezomib did not inhibit HDAC activity like conventional HDAC inhibitors but down-regulated the expression of class I HDACs, because we and others have shown that bortezomib suppressed the expressions of various molecules, such as CD49d,[30] HLA class I,[36] and DNMT1,[37] in MM cells. To verify this hypothesis, we determined the expression of class I HDACs (HDAC1, HDAC2, and HDAC3) in human MM cell lines (KMS12-BM, U266, and RPMI8226) during bortezomib treatment. We also treated MM cell lines with conventional antimyeloma drugs (vincristine, dexamethasone, and doxorubicin) to be used as control samples. As shown in Figure 2A, along with the induction of histone hyperacetylation, bortezomib readily down-regulated the expression of class I HDACs in all 3 MM cell lines. In contrast, there were no significant changes in histone acetylation and HDAC expression in cells treated with other drugs. The histone hyperacetylation and down-regulation of HDACs were reciprocally induced by bortezomib in a dose- and time-dependent fashion (Figure 2B-C). These results suggest that bortezomib induced histone hyperacetylation via the down-regulation of class I HDACs expression in MM cells.

Next, we determined whether the down-regulation of HDAC expression occurred at transcriptional or posttranscriptional levels. We performed semiquantitative RT-PCR and real-time quantitative RT-PCR in MM cells during bortezomib treatment. As shown in Figure 2D-E, bortezomib down-regulated mRNA levels of HDAC1, HDAC2, and HDAC3 in all 3 MM cell lines in a time-dependent fashion. The suppression pattern was quite similar to that of proteins. In addition, semiquantitative RT-PCR and Western blot analyses revealed that there were no significant changes in the expression of other classes of HDACs, such as HDAC4, HDAC5, HDAC6, and SIRT1 (supplemental Figure 2; data not shown). These results suggest that bortezomib transcriptionally repressed the expression of class I HDACs in MM cells.

In addition, we performed the same experiments using primary myeloma cells: $CD138^+$ cells from BM mononuclear cells of patients with MM. First, primary MM cells (patient no. 3) were cultured in the absence or presence of 2, 4, and 8nM bortezomib for 2 days, followed by semiquantitative RT-PCR analysis. We could detect HDAC1, HDAC2, and HDAC3 transcripts in a semiquantitative manner between 30 and 40 PCR cycles (supplemental Figure 3A), and observed the down-regulation of HDAC expression at more than 2 nM bortezomib (supplemental Figure 3B-C). Based on these preliminary experiments, we cultured primary MM cells in the absence or presence of 2nM bortezomib for 2 days and detected the expression of HDAC genes at 40 PCR cycles. As shown in Figure 2F and G, bortezomib significantly down-regulated the expressions of HDAC1, HDAC2, and HDAC3 in primary myeloma cells, suggesting that bortezomib transcriptionally down-regulated the expressions of class I HDACs in primary MM cells as well as cell lines.

Caspase-8–dependent cleavage of Sp1 protein underlies transcriptional repression of HDAC genes by bortezomib

Next, we investigated the mechanisms of transcriptional repression of HDAC genes during bortezomib treatment in MM cells. As illustrated in Figure 3A, there are a number of putative transcription factor binding sites in the promoter regions of class I HDAC genes. We have previously shown that Sp1 and GATA1 are potent transcriptional activators, and MZF-1, GATA2, and C/EBPα are repressors for HDAC1 transcription in myeloid cells.[15] We initially screened for the expression of these factors in MM cells, and identified the expression of Sp1 and MZF-1 but not GATA1, GATA2 and C/EBPα (Figure 3B; data not shown). Therefore, we focused on Sp1 and MZF-1 as transcriptional regulators of HDACs in MM cells. Because their binding sites are commonly observed in the promoter regions of 3 HDAC genes, we speculated that HDAC transcription was regulated in a similar manner in MM cells. First, we examined the transcriptional activity of the HDAC1 promoter in KMS12-BM cells by reporter assays using the segment between −1179 and +397 of the HDAC1 gene, which confers full promoter activity.[15] As shown in Figure 3C, overexpression of Sp1 significantly increased HDAC1 promoter activity, whereas MZF-1 failed to do so, indicating that Sp1 acts as a transcriptional activator in KMS12-BM cells. In addition, bortezomib was shown to modify the transcriptional activity in this system (Figure 3C). We also examined the transcriptional activity of the HDAC3 promoter in KMS12-BM cells. Reporter assays revealed that promoter activity was enhanced by Sp1 but not MZF-1, suggesting that Sp1 transactivates HDAC3 as well as HDAC1 (data not shown). Furthermore, bortezomib also reduced HDAC3 promoter activity (data not shown). Taken together, Sp1 is a major transcriptional activator of class I HDAC genes in MM cells.

Figure 3. Regulation of HDAC1 promoter by Sp1 transcription factor. (A) Schematic representations of HDAC1, HDAC2, and HDAC3 promoter constructs are shown. Relative locations of the putative binding sites of hematopoietic transcription factors are approximated by the symbols shown in the box. (B) Whole-cell lysates were prepared from MM cell lines and subjected to immunoblotting. HEK293 cells were transduced with expression vectors encoding Sp1, MZF-1, and C/EBPα, and used as positive controls. (C) We transfected 10 μg of pGL4.10 plasmid containing HDAC1 promoter sequences between −1170 and +397 into KMS12-BM cells along with 10 μg of expression vectors encoding Sp1 and MZF-1, and measured luciferase activities after 48 hours. HDAC1 promoter activity was calculated as firefly luciferase activities of cells transfected with an empty expression vector set at 1.0 after normalization of transfection efficiencies using Renilla luciferase activities. Data shown are the means ± SD of 3 independent experiments. *P* values were calculated by 1-way ANOVA with Student-Newman-Keuls multiple comparisons test. **P* < .05. (D) KMS12-BM cells were cultured in the absence or presence of bortezomib for 2 days and subjected to ChIP assays. Chromatin suspensions were immunoprecipitated with the indicated antibodies and corresponding control antibodies. The resulting precipitants were subjected to PCR to amplify the promoter regions of the HDAC genes. The amplified products were visualized by ethidium bromide staining after 2% agarose gel electrophoresis. Representative data of 50 cycles are shown. Input indicates that PCR was performed with genomic DNA. (E) Whole-cell lysates were isolated simultaneously in the experiments described in Figure 2C, and subjected to immunoblotting. Arrows "a" and "b" indicate the intact and cleaved bands of Sp1, respectively. The signal intensities of each band were quantified, normalized to those of the corresponding GAPDH, and shown as relative values setting day 0 controls to 1.0. (F) KMS12-BM cells were cultured with the indicated combinations of 8nM bortezomib (Bort), 100μM z-IETD-FMK (caspase-8 inhibitor), 100μM z-LEHD-FMK (caspase-9 inhibitor), 50μM z-DEVD-FMK (caspase-3 inhibitor), and 20μM z-ATAD-FMK (caspase-12 inhibitor) for 48 hours. Whole-cell lysates were subjected to immunoblotting. (G) Cell viability was determined with a Cell Counting Kit (WAKO) after culturing MM cells in the absence or presence of 8nM bortezomib (Bort) with or without either 100μM z-IETD-FMK (IETD) or 100μM z-LEHD-FMK (LEHD) for 48 hours. Absorbance at 450 nm was measured with a microplate reader, and expressed as a percentage of the value of the corresponding untreated cells. The means ± SD (bars) of 3 independent experiments are shown. *P* values were calculated by 1-way ANOVA with the Student-Newman-Keuls multiple comparisons test. **P* < .05.

Next, we performed ChIP assays to investigate the binding of these transcriptional regulators to HDAC promoters in vivo and their changes during bortezomib treatment. We detected the binding of Sp1 to HDAC1, HDAC2, and HDAC3 promoter regions in untreated KMS12-BM cells, whereas Sp1 dissociated from all 3 promoters upon bortezomib treatment (Figure 3D). Although MM cells expressed MZF-1, we could not detect its binding to promoters. These results suggest that Sp1 confers the baseline expression of HDAC genes.

To clarify the mechanisms of changes in promoter binding, we detected the expression of Sp1 protein in MM cell lines during bortezomib treatment. As shown in Figure 3E, bortezomib markedly down-regulated the expression of Sp1 in all 3 MM cell lines in a time-dependent fashion. In addition, we found that an extra signal (indicated by arrow "b" in Figure 3E) appeared below the major signal of Sp1 protein (indicated by arrow "a" in Figure 3E) in bortezomib-treated cells. Previous studies showed that Sp1 protein was cleaved and degraded by caspases such as caspase-8, caspase-9, and caspase-3,[38] and bortezomib activated caspase-8, caspase-9, caspase-3, and caspase-12.[39-41] On this basis, we hypothesized that the extra signal was caspase-cleaved Sp1 protein. To confirm this hypothesis, we cultured KMS12-BM cells with peptide inhibitors of caspase-8 (z-IETD-FMK), caspase-9 (z-LETD-FMK), caspase-3 (z-DEVD-FMK), and caspase-12 (z-ATAD-FMK) in the absence or presence of bortezomib, and examined the expression of Sp1 protein. As shown in Figure 3F, IETD but not other inhibitors perturbed the bortezomib-induced down-regulation of Sp1. In KMS12-BM cells, caspase-8 activation occurred 12 hours after bortezomib exposure, which was accompanied by reciprocal down-regulation of Sp1 expression (supplemental Figure 4). These results suggest that caspase-8 is responsible for the cleavage and degradation of Sp1 protein in bortezomib-treated cells. In parallel with the restored Sp1 expression, the caspase-8 inhibitor blocked the down-regulation of HDAC expression in KMS12-BM cells. In addition, IETD but not other caspase inhibitors could abrogate bortezomib-induced cytotoxicity in KMS12-BM cells in a dose-dependent fashion (Figure 3G; supplemental Figure 5). These results suggest that bortezomib degraded Sp1 protein via the caspase-8–dependent pathways, leading in turn to the transcriptional repression of HDAC genes in MM cells. In line with our observation, Hideshima et al[39] reported that caspase-8 is a primary initiating caspase in bortezomib-mediated cell death. Taken together, our results suggest that the caspase-8/Sp1/HDAC axis is a critical pathway for bortezomib-mediated cytotoxicity in MM cells.

Increased cytotoxicity of bortezomib by shRNA/siRNA-mediated knockdown of HDAC1 expression

To confirm the roles of HDACs in bortezomib-induced cytotoxicity, we performed loss-of-function analysis using the shRNA/siRNA lentivirus system.[30] We could achieve significant loss-of-function of HDACs by solely targeting HDAC1, because HDAC1 represents more than half of all cellular HDAC activities, and other HDACs cannot compensate for the loss of HDAC1.[11] We constructed lentiviral shRNA/siRNA expression vectors (supplemental Figure 6A) and transfected them into 3 MM cell lines for further analyses. As shown in Figure 4A, specific reduction of HDAC1 expression was confirmed by Western blotting in GFP$^+$ cells collected by a cell sorter. Upon transduction with shRNA, we determined apoptosis induction in the absence or presence of bortezomib. As shown in Figure 4B, HDAC1 knockdown slightly increased apoptosis in untreated MM cells, but the effect was not statistically significant compared with inactive sh-controls. With bortezomib treatment, however, HDAC1 knockdown significantly increased apoptosis in 3 MM cell lines; this effect was observed at various doses of bortezomib (supplemental Figure 7A). Cell proliferation assays and BrdU/7-AAD double staining revealed that HDAC1 knockdown only marginally affected growth rate and cell-cycle patterns (supplemental Figure 7B-C). These results

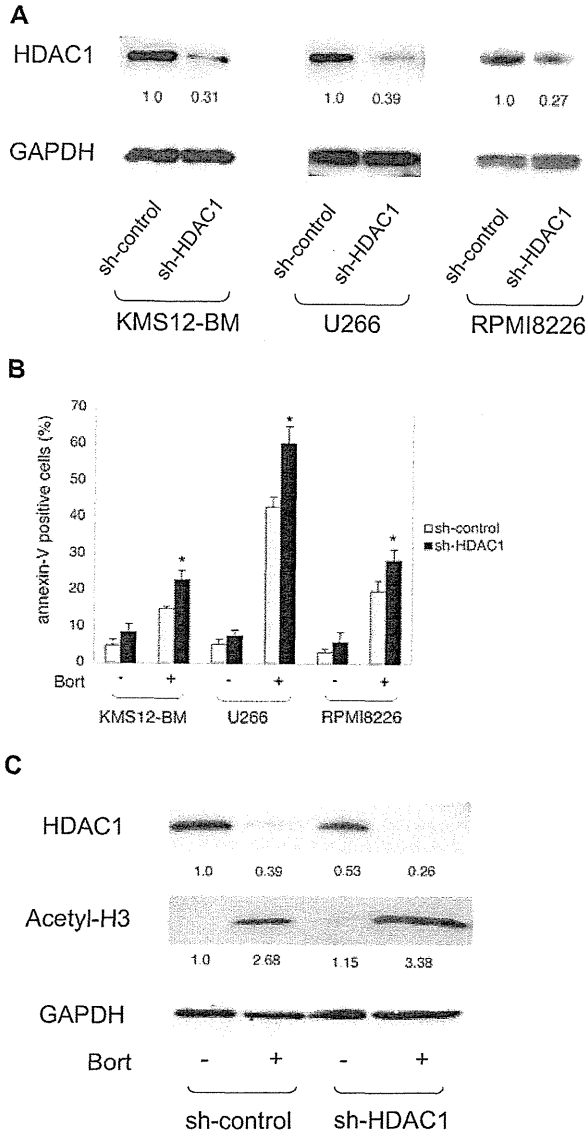

Figure 4. Effects of shRNA-mediated knockdown of HDAC1 on bortezomib-induced apoptosis in MM cells. (A) MM cell lines were transfected with either pLL3.7-sh-HDAC1 (sh-HDAC1) or sh-control vector. Whole-cell lysates were prepared from GFP$^+$ cells collected using a FACSAria flow cytometer and subjected to immunoblotting. The signal intensities of each band were quantified, normalized to those of the corresponding GAPDH, and shown as relative values setting the sh-control to 1.0. (B) MM cell lines transfected with shRNA vectors were cultured in the absence or presence of 2nM bortezomib. After 48 hours, MM cells were harvested, stained with annexin-V/APC, and subjected to flow cytometric analysis. The y-axis shows the proportion of annexin-V positivity in the GFP$^+$ fraction. The means ± SD (bars) of 3 independent experiments are shown. *P* values were calculated by 1-way ANOVA with the Student-Newman-Keuls multiple comparisons test. $^*P < .05$ against the sh-control. (C) shRNA-transduced RPMI8226 cells were cultured in the absence or presence of 2nM bortezomib. After 48 hours, whole-cell lysates were prepared from GFP$^+$ cells collected by the FACSAria flow cytometer, and subjected to immunoblotting. The signal intensities of each band were quantified, normalized to those of the corresponding GAPDH, and shown as relative values setting the untreated sh-control to 1.0.

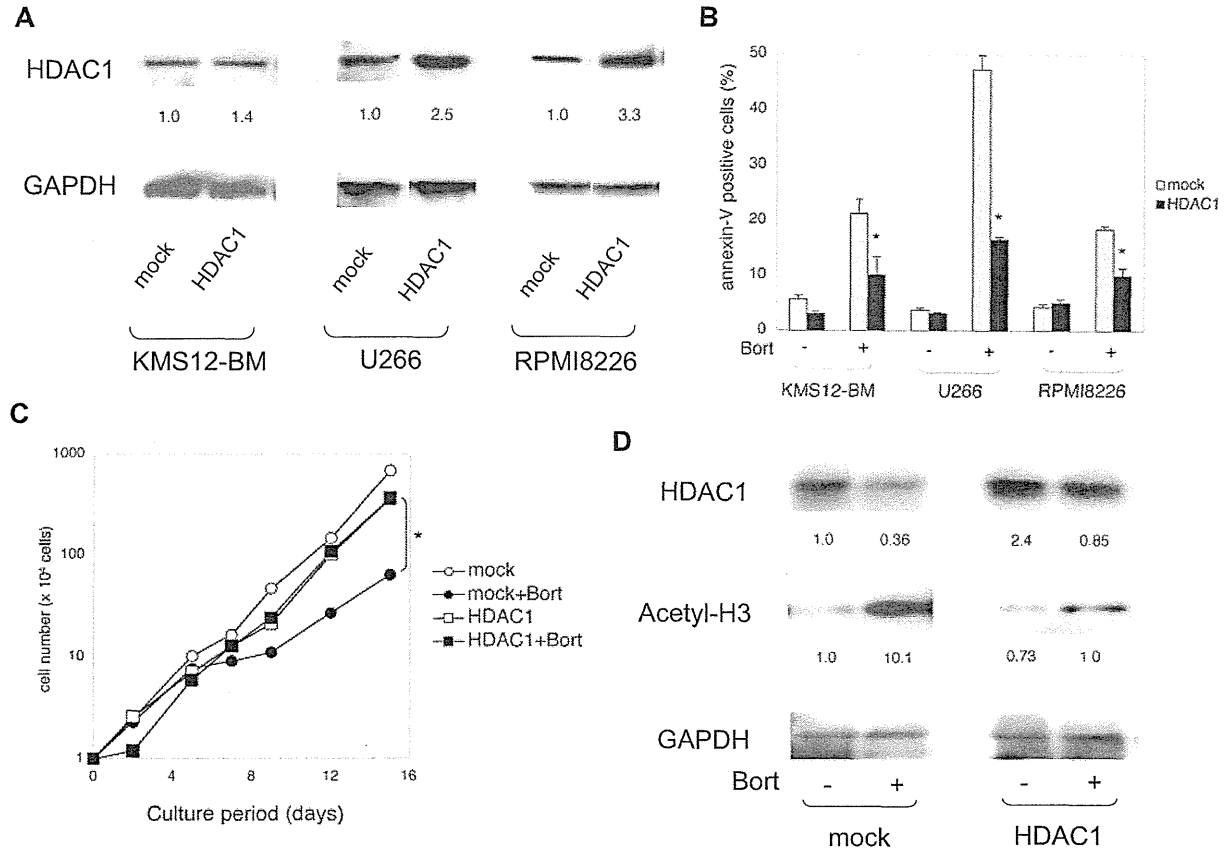

Figure 5. Effects of HDAC1 overexpression on bortezomib-induced apoptosis in MM cells in vitro. (A) MM cell lines were lentivirally transfected with CSII-DsRed (mock) or CSII-DsRed-HDAC1 (HDAC1) vector. Whole-cell lysates were prepared from DsRed$^+$ cells collected using a FACSAria flow cytometer and subjected to immunoblotting. The signal intensities of each band were quantified, normalized to those of the corresponding GAPDH, and shown as relative values with mock-transfected controls setting to 1.0. (B) MM cell lines transfected with mock or HDAC1 vector were cultured in the absence or presence of 2nM bortezomib. After 48 hours, MM cells were harvested, stained with annexin-V/APC, and subjected to flow cytometric analysis. The y-axis shows the proportion of annexin-V positivity in the DsRed$^+$ fraction. The means ± SD (bars) of 3 independent experiments are shown. *P* values were calculated by 1-way ANOVA with the Student-Newman-Keuls multiple comparisons test. **P* < .05 against the mock. (C) RPMI 8226 cells transfected with mock or HDAC1 vector were cultured in the absence or presence of 2nM bortezomib. Total numbers of DsRed$^+$ cells were calculated by flow cytometer at the indicated time points. *P* values were calculated by 1-way ANOVA with the Student-Newman-Keuls multiple comparisons test. **P* < .05 against the mock + Bort. (D) After 48 hours, whole-cell lysates were prepared from DsRed$^+$ cells collected using a FACSAria flow cytometer and subjected to immunoblotting. The signal intensities of each band were quantified, normalized to those of the corresponding GAPDH, and shown as relative values with untreated mock-transfected controls setting to 1.0.

indicate that the consequence of HDAC down-regulation is mainly apoptosis induction rather than growth inhibition. Histone hyperacetylation was enhanced by HDAC1 knockdown in bortezomib-treated RPMI8226 cells (Figure 4C). Therefore, it appears that shRNA-mediated knockdown of HDAC1 increases sensitivity to bortezomib via synergistic inhibition of HDAC activity in MM cells. These results suggest that bortezomib-induced cytotoxicity depends on cellular HDAC activities in MM cells.

HDAC1 overexpression rescues MM cells from bortezomib-induced apoptosis

To confirm the dependency of bortezomib action on HDACs, we performed gain-of-function of HDAC1 in MM cells using the lentiviral transduction system (supplemental Figure 6B).[27] CSII-DsRed (mock) and CSII-HDAC1-DsRed (HDAC1) vectors were lentivirally transduced into 3 MM cell lines. HDAC1 overexpression was confirmed by Western blotting in DsRed$^+$ cells collected by a cell sorter (Figure 5A). Using this system, we examined the effects of HDAC1 overexpression on bortezomib-induced apoptosis. As shown in Figure 5B, there was no significant difference in the proportion of apoptosis between mock- and HDAC1-transduced cells in the absence of bortezomib. In contrast, bortezomib-induced apoptosis was significantly inhibited by HDAC1 overexpression. The inhibition of apoptosis was observed in increased doses of bortezomib (supplemental Figure 8). However, overexpression of HDAC2 and HDAC3 did not ameliorate the effect of the drug (supplemental Figure 9), suggesting that the HDAC1 levels determine the sensitivity to bortezomib. Next, we investigated the effect of HDAC1 overexpression on the growth of bortezomib-treated cells. As shown in Figure 5C, there was no significant difference in the growth rate between mock- and HDAC1-transduced RPMI8226 cells in the absence of bortezomib. In the presence of bortezomib, the growth of mock-transduced cells was significantly delayed due to the induction of apoptosis. In contrast, HDAC1-transduced cells grew as fast as untreated cells, suggesting that HDAC1 overexpression ameliorates the cytotoxic effects of bortezomib. In addition, we examined the status of histone acetylation in these cells. As anticipated, HDAC1 overexpression markedly diminished bortezomib-induced hyperacetylation of histones (Figure 5D) but not tubulin (supplemental Figure 11). Taken together, HDAC1 overexpression rescued MM cells from bortezomib-induced apoptosis by sustaining HDAC activity in MM cells.

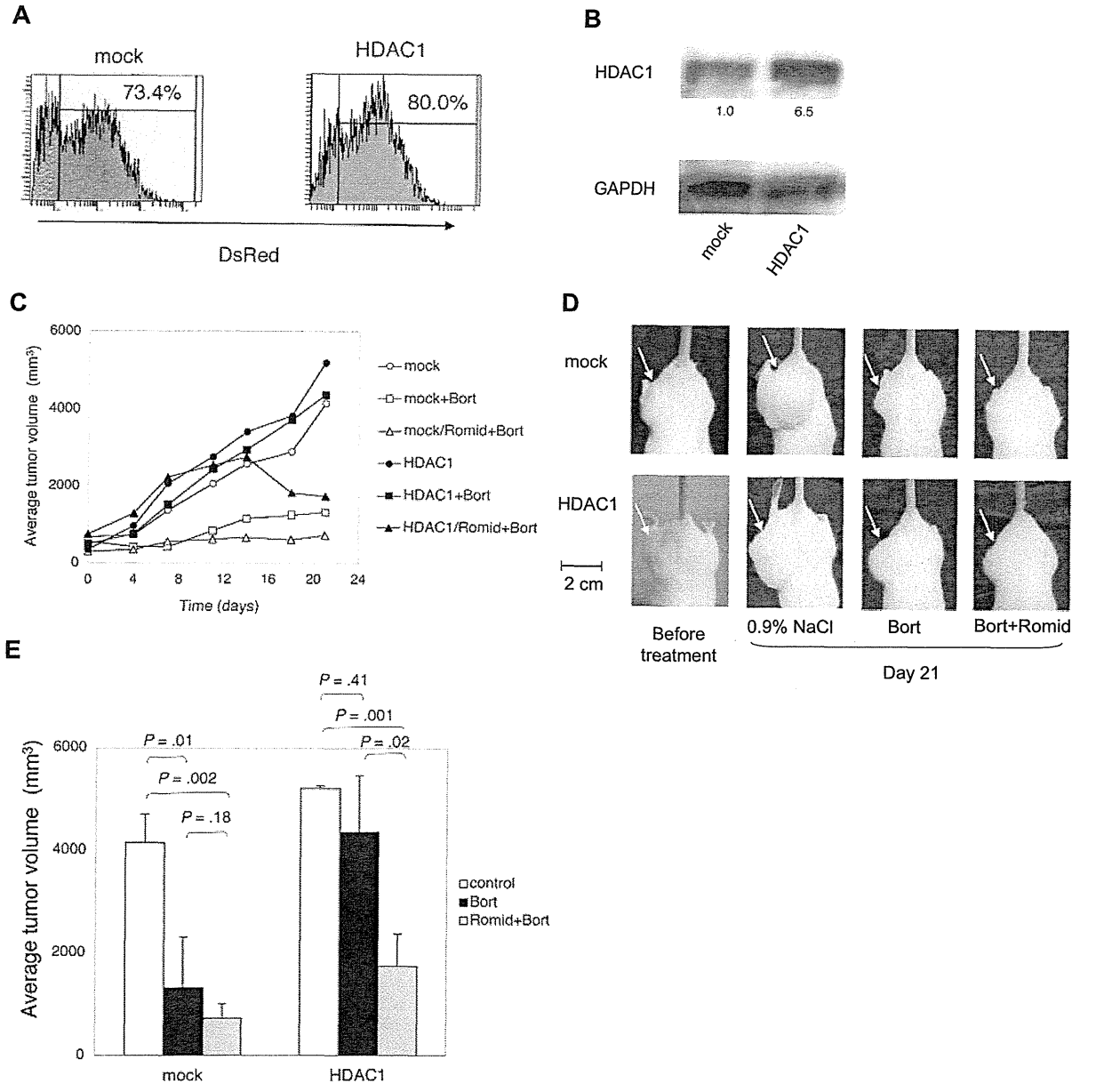

Figure 6. Effects of HDAC1 overexpression on bortezomib-induced apoptosis in RPMI 8226 cells in vivo. (A) RPMI 8226 cells were transfected with CSII-DsRed (mock) or CSII-DsRed-HDAC1 (HDAC1) vector. DsRed$^+$ cells were collected using a FACSAria flow cytometer and seeded 1 cell/well in a 96-well plate; single-cell clones were then obtained. Each subline was analyzed by a flow cytometer, and representative histogram plots of whole cells are shown. (B) Whole-cell lysates were subjected to immunoblotting. The signal intensities of HDAC1 were quantified, normalized to those of the corresponding GAPDH, and shown as relative values. (C) NOD/SCID mice were inoculated subcutaneously with 3×10^7 cells of RPMI 8226 sublines in the right thigh. The following treatments were started at day 0 when tumors were measurable: bortezomib intravenously twice a week, romidepsin intraperitoneally every other day, and vehicle (0.9% NaCl) alone at the same schedule. Caliper measurements of the longest perpendicular tumor diameters were performed on alternate days to estimate the tumor volume (mm^3) using the following formula: $4/3\pi \times (\text{width}/2)^2 \times (\text{length}/2)$. Mice inoculated with mock clones were treated with vehicle alone (mock; ○; n = 5), 0.5 mg/kg bortezomib (mock + Bort; □; n = 4), or 0.5 mg/kg bortezomib and 0.25 mg/kg romidepsin (HDAC1/Romid + Bort; △; n = 4). Mice inoculated with HDAC1 clones were treated with vehicle alone (HDAC1; ●; n = 4), 0.5 mg/kg bortezomib (HDAC1 + Bort; ■; n = 3), or 0.5 mg/kg bortezomib and 0.25 mg/kg romidepsin (HDAC1/Romid + Bort; ▲; n = 4). (D) Representative photographs of inoculated NOD/SCID mice at day 21 are shown (original magnification, ×2). Arrowheads indicate inoculated tumors. (E) The y-axis shows the tumor volume in inoculated mice at day 21. The means ± SD (bars) are shown. *P* values were calculated by 1-way ANOVA with the Student-Newman-Keuls multiple comparisons test.

Bortezomib resistance of HDAC1-transduced MM cells in NOD/SCID mice

Finally, we confirmed the role of HDACs as target molecules of bortezomib in vivo. To this end, we established RPMI 8226 sublines lentivirally transduced with CSII-DsRed (mock) or CSII-HDAC1-DsRed (HDAC1). Whereas each subline expressed DsRed at equal levels (Figure 6A), HDAC1 was overexpressed solely in the HDAC1-transduced subline (Figure 6B). We inoculated them subcutaneously into nonobese diabetic/severe combined immunodeficiency (NOD/SCID) mice in the right thigh at 3×10^7 cells.[31] When measurable tumors developed after 10 to 14 days, mice were assigned to 3 groups: vehicle (0.9% NaCl) control, 0.5 mg/kg bortezomib–treated, and 0.25 mg/kg romidepsin and 0.5 mg/kg bortezomib–treated (n = 3-5 in each group). As shown in Figure 6C, tumor volume constantly increased in vehicle control mice given transplants of both mock and HDAC1 until 21 days. Bortezomib strikingly inhibited tumor growth in mice